

NAVAL POSTGRADUATE SCHOOL

Monterey, California



THESIS

**VALIDATION OF A STOCHASTIC BOUSSINESQ MODEL FOR
WAVE SPECTRA TRANSFORMATION IN THE SURF ZONE**

by

Marianie O. Balolong

March 2001

Thesis Advisor:
Second Reader:

T.H.C Herbers
Edward B. Thornton

Approved for public release; distribution is unlimited

20010627 073

REPORT DOCUMENTATION PAGE			Form Approved OMB No. 0704-0188	
Public reporting burden for this collection of information is estimated to average 1 hour per response, including the time for reviewing instruction, searching existing data sources, gathering and maintaining the data needed, and completing and reviewing the collection of information. Send comments regarding this burden estimate or any other aspect of this collection of information, including suggestions for reducing this burden, to Washington headquarters Services, Directorate for Information Operations and Reports, 1215 Jefferson Davis Highway, Suite 1204, Arlington, VA 22202-4302, and to the Office of Management and Budget, Paperwork Reduction Project (0704-0188) Washington DC 20503.				
1. AGENCY USE ONLY (Leave blank)		2. REPORT DATE March 2001	3. REPORT TYPE AND DATES COVERED Master's Thesis	
4. TITLE AND SUBTITLE: Title (Mix case letters) Validation of a Stochastic Boussinesq Model for Wave Spectra Transformation in the Surf Zone.			5. FUNDING NUMBERS	
6. AUTHOR(S) Marianne O. Balolong				
7. PERFORMING ORGANIZATION NAME(S) AND ADDRESS(ES) Naval Postgraduate School Monterey, CA 93943-5000			8. PERFORMING ORGANIZATION REPORT NUMBER	
9. SPONSORING / MONITORING AGENCY NAME(S) AND ADDRESS(ES) N/A			10. SPONSORING / MONITORING AGENCY REPORT NUMBER	
11. SUPPLEMENTARY NOTES The views expressed in this thesis are those of the author and do not reflect the official policy or position of the Department of Defense or the U.S. Government.				
12a. DISTRIBUTION / AVAILABILITY STATEMENT Approved for public release; distribution is unlimited.			12b. DISTRIBUTION CODE	
13. ABSTRACT (maximum 200 words) <p>This thesis presents a field validation of a stochastic, nonlinear wave shoaling model based on a third-order closure Boussinesq equations (Herbers and Burton, 1997). The model predicts the evolution of directionally spread waves propagating over an alongshore uniform beach. The model consists of a coupled set of evolution equations for the wave spectrum and bispectrum that incorporates linear shoaling and refraction effects and nonlinear energy exchanges in near-resonant triad interactions. Dissipation due to breaking is approximated using an empirical quasi-linear damping function and a relaxation to Gaussian statistics. The model was verified with field data from five alongshore instrument arrays deployed near Duck, North Carolina from August to December 1997 as part of the SandyDuck experiment. The predicted shoaling evolution of the frequency-directional wave spectra shows the expected development of harmonic peaks through triad interactions. The predicted harmonic spectral levels and direction are in good agreement with the observed spectra, but the predicted directional spread is biased low inside the surf zone. The significant wave height predictions are generally in good agreement with observations. The model tends to overshoot the waves outside the surf zone and slightly overdisperse wave energy inside the surf zone. Infragravity wave growth, sea surface skewness and asymmetry are predicted fairly accurately by the model.</p>				
14. SUBJECT TERMS Stochastic Boussinesq Wave Model, Ocean Surface Gravity Waves, Frequency-Directional Wave Spectra, Surf Zone, Wave Shoaling, Beach			15. NUMBER OF PAGES 74	
			16. PRICE CODE	
17. SECURITY CLASSIFICATION OF REPORT Unclassified	18. SECURITY CLASSIFICATION OF THIS PAGE Unclassified	19. SECURITY CLASSIFICATION OF ABSTRACT Unclassified	20. LIMITATION OF ABSTRACT UL	

THIS PAGE INTENTIONALLY LEFT BLANK

Approved for public release; distribution unlimited.

**VALIDATION OF A STOCHASTIC BOUSSINESQ MODEL FOR
WAVE SPECTRA TRANSFORMATION IN THE SURF ZONE**

Marianie O. Balolong
Lieutenant, United States Navy
B.S., Jacksonville University, 1996

Submitted in partial fulfillment of the
requirements for the degree of

**MASTER OF SCIENCE IN METEOROLOGY AND PHYSICAL
OCEANOGRAPHY**

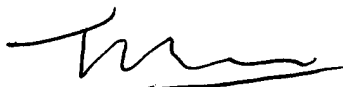
from the

**NAVAL POSTGRADUATE SCHOOL
March 2001**

Author:

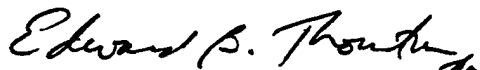

Marianie O. Balolong

Approved by:


T.H.C. Herbers, Thesis Advisor



Edward B. Thornton, Second Reader



Roland W. Garwood, Chairman
Department of Oceanography

THIS PAGE INTENTIONALLY LEFT BLANK

ABSTRACT

This thesis presents a field validation of a stochastic, nonlinear wave shoaling model based on a third-order closure Boussinesq equations (Herbers and Burton, 1997). The model predicts the evolution of directionally spread waves propagating over an alongshore uniform beach. The model consists of a coupled set of evolution equations for the wave spectrum and bispectrum that incorporates linear shoaling and refraction effects and nonlinear energy exchanges in near-resonant triad interactions. Dissipation due to breaking is approximated using an empirical quasi-linear damping function and a relaxation to Gaussian statistics. The model was verified with field data from five alongshore instrument arrays deployed near Duck, North Carolina from August to December 1997 as part of the SandyDuck experiment. The predicted shoaling evolution of the frequency-directional wave spectra shows the expected development of harmonic peaks through triad interactions. The predicted harmonic spectral levels and direction are in good agreement with the observed spectra, but the predicted directional spread is biased low inside the surf zone. The significant wave height predictions are generally in good agreement with observations. The model tends to overshoot the waves outside the surf zone and slightly overdissipate wave energy inside the surf zone. Infragravity wave growth, sea surface skewness and asymmetry are predicted fairly accurately by the model.

THIS PAGE INTENTIONALLY LEFT BLANK

TABLE OF CONTENTS

I.	INTRODUCTION.....	1
II.	FIELD EXPERIMENT AND DATA ANALYSIS	5
III.	MODEL DESCRIPTION AND IMPLEMENTATION	11
IV.	CASE STUDIES.....	15
	CASE I: AUGUST 7, 1997 01:00 EST.....	16
	CASE II: AUGUST 10, 1997 04:00 EST	17
	CASE III: SEPTEMBER 12, 1997 07:00 EST	18
	CASE IV: OCTOBER 19, 1997 16:00 EST.....	19
V.	OVERALL MODEL PERFORMANCE.....	21
VI.	SUMMARY	27
	LIST OF REFERENCES	53
	INITIAL DISTRIBUTION LIST.....	55

THIS PAGE INTENTIONALLY LEFT BLANK

LIST OF FIGURES

Figure 1.	Bathymetry at the field site surveyed on September 16, 1997. The instrumented region is indicated with a red box. The trench located to the south of the instrumented region is caused by the presence of a 600m-long pier.....	31
Figure 2.	Plan View of Arrays. Instrument types include SPUV (collocated sonar, pressure sensor, and current meter), PUV (collocated pressure sensor and current meter) and P (pressure sensor). In this study 5 alongshore arrays of pressure sensors (labeled B, C, E, F, and 8m arrays, sensors indicated in blue) are used	31
Figure 3.	Three-dimensional view of pressure sensor arrays used in this study.....	32
Figure 4.	Sonar Altimeter Locations.	32
Figure 5.	Comparison of beach profiles obtained from CRAB and sonar altimeter data. The sonar measurements (asterisks) were interpolated linearly, except over the sand bar where a cubic spline was used. (a) small wave conditions. (b) storm conditions.....	33
Figure 6.	(a) Evolution of offshore H_s (measured in 8m depth) during the four month deployment. (b) Root-mean-square difference between beach profile based on CRAB and sonar altimeter data. Vertical dashed lines indicate times of beach profiles shown in figure 5.....	34
Figure 7.	Frequency and frequency-directional spectra for Case I, (August 7, 1997 01:00 EST). The top panels display the (direction-integrated) frequency spectra at each array (blue line is model prediction, red line is observed spectrum at that array). The middle and lower panels contain the observed and predicted frequency-directional spectra, respectively. Note the exclusion of high frequency, large angle waves from the initializing model spectrum at the F array.....	35
Figure 8.	Case I, cross-shore shoaling evolution of significant wave height H_s , asymmetry, and skewness. Predictions of model runs initialized in 8m (dashed) and 5m (solid) depths are compared to observations (*) at each array. The depth profile and array locations are shown in bottom panel.....	36
Figure 9.	Case I, cross-shore shoaling evolution of infragravity variance, mean direction, and directional spread. Predictions of model runs initialized in 8m (dashed) and 5m (solid) depths are compared to observations (*) at each array. The depth profile and array locations are shown in bottom panel.....	37
Figure 10.	Frequency and frequency-directional spectra for Case II, (August 10, 1997 04:00 EST) (same format as figure 7).	38
Figure 11.	Case II, cross-shore shoaling evolution of significant wave height H_s , asymmetry, and skewness (same format as figure 8).	39
Figure 12.	Case II, cross-shore shoaling evolution of infragravity variance, mean direction, and directional spread (same format as figure 9).....	40

Figure 13.	Frequency and frequency directional spectra for Case III (September 12, 1997 07:00 EST) (same format as figure 7). In order to enhance the directional properties at higher frequencies, the frequency-directional spectra (bottom two panels) were multiplied by the frequency.	41
Figure 14.	Case III, cross-shore shoaling evolution of significant wave height H_s , asymmetry, and skewness (same format as figure 8).	42
Figure 15.	Case III, cross-shore shoaling evolution of infragravity variance, mean direction, and directional spread (same format as figure 9).	43
Figure 16.	Frequency and frequency-directional spectra for Case IV (October 19, 1997 16:00 EST) (same format as figure 7). Note the exclusion of high frequency, large angle waves from the initializing model spectrum at the F array. In order to enhance the directional properties at higher frequencies, the frequency-directional spectra (bottom two panels) were multiplied by the frequency.	44
Figure 17.	Case IV, cross-shore shoaling evolution of significant wave height H_s , asymmetry, and skewness (same format as figure 8).	45
Figure 18.	Case IV: cross-shore shoaling evolution of infragravity variance, mean direction, and directional spread (same format as figure 9).	46
Figure 19.	Left panels: predicted versus observed significant wave height (H_s) at the E, C, and B arrays. The model was initialized at the F array. Right panels: predicted versus observed significant wave height (H_s) both normalized by the initial H_s value. Solid diagonal line indicates a one-to-one correspondence, dashed line is a linear regression fit to all data points. .	47
Figure 20.	Predicted versus observed infragravity variance, both normalized by the initial infragravity variance. Left panels: results at the F, E, C, and B arrays for model runs initialized at the 8m array. Right panels: results at the E, C, and B arrays for model runs initialized at the F array. Solid diagonal line indicates a one-to-one correspondence, dashed line is a linear regression fit to all data points.	48
Figure 21.	Predicted versus observed skewness (left panels) and asymmetry (right panels) at the E, C, and B arrays. The model was initialized at the F array. Solid diagonal line indicates a one-to-one correspondence, dashed line is a linear regression fit to all data points.	49
Figure 22.	Predicted versus observed mean direction (left panels) and directional spread (right panels) at the E, C, and B arrays. The model was initialized at the F array. Solid diagonal line indicates a one-to-one correspondence, dashed line is a linear regression fit to all data points.	50

LIST OF TABLES

Table 1.	Error statistics for model predictions initialized at the 8m array. Results are included from the F,E,C, and B arrays.	51
Table 2.	Error statistics for model predictions initialized at the F array. Results are included from the E,C, and B arrays.	51

THIS PAGE INTENTIONALLY LEFT BLANK

ACKNOWLEDGMENTS

Wave and seabed level measurements in depths less than 5m were collected by Drs. Steve Elgar (Woods Hole Oceanographic Institution) and Robert T. Guza (Scripps Institution of Oceanography). Wave measurements in 8m depth and bathymetry surveys were collected by the U.S. Army Engineer Field Research Facility, Duck, NC.

Permission to use these data is appreciated.

Sincere gratitude is extended to my advisor, Thomas H.C. Herbers, for his guidance and patience throughout this thesis process. Edward B. Thornton for graciously accepting to be my second reader. Mark Orzech for his mentorship concerning the model and sincere concern for the completion of this thesis. Paul Jessen provided exceptional technical and software assistance. Arlene Guest, Mike Cook, Donna Burych, Bob Creasy, Bill Thompson, and Mary Jordan provided excellent computer advice.

I would like to thank my parents, Antonio and Angelita Balolong, for instilling a strong work ethic and a foundation of faith in me.

I would like to thank my wife, Marilyn, for her undying love and encouragement. She brings out the best in me.

I. INTRODUCTION

The focus of this thesis is the verification of a new stochastic Boussinesq wave model for the transformation of random surface waves across a natural beach (Herbers and Burton, 1997, Herbers et al; manuscript in preparation). Accurate predictions of wave shoaling transformation are important for both military (e.g., the planning of successful U.S. naval amphibious operations) and civilian (e.g. predicting beach erosion during storms) applications. Both linear and nonlinear processes affect the characteristics of ocean waves as they shoal onto beaches. Well-established linear theory predicts the increase of wave amplitudes, the decrease of wavelengths, and refraction of propagation directions toward normal incidence. Changes in directional characteristics of waves are particularly important for wave-driven longshore currents and sediment transport in the surf zone. In shallow water, nonlinear effects become pronounced, transforming initially symmetric, sinusoidal wave profiles to asymmetric, pitched forward profiles of near-breaking waves. Near-resonant nonlinear interactions between triads of wave components transfer energy from the incident wave components to higher-frequency (harmonic) and lower-frequency (infragravity) components. These interactions not only broaden the wave spectrum, but also phase-couple the spectral components causing the characteristic steepening and pitched-forward profiles of near-breaking waves (e.g., Freilich and Guza, 1984; Elgar and Guza, 1985), and skewed near-bed velocity profiles that are believed to play an important role in cross-shore sediment transport. This nonlinear evolution process is described well by depth-integrated Boussinesq equations for weakly nonlinear, weakly dispersive waves in varying depth (Peregrine, 1967). Time-domain Boussinesq models can be applied in principle to natural beaches with

arbitrary incident wave conditions, but obtaining complete solutions is computationally expensive for large domains and requires detailed boundary conditions that are often unavailable. So far, practical applications have been mostly restricted to 1-D implementations for uni-directional waves.

Recently, stochastic models for the transformation of random waves on a beach have been developed that solve evolution equations for statistically averaged spectral wave properties (e.g., Abreu et al., 1992; Eldeberky and Battjes, 1996; Agnon and Sheremet, 1997; Herbers and Burton, 1997). These models are numerically efficient and can be initialized with wave spectra at an offshore boundary, which are easily obtained from routine wave measurements or regional wave model predictions. However, stochastic models require a statistical closure that may result in significant errors for long propagation distances and areas of strong nonlinearity.

Whereas several theories exist for nonlinear wave interactions, the wave breaking process in the surf zone is not yet fully understood and must be described by heuristic models. The majority of random wave breaking models are based on the analogy of individual wave crests with turbulent bores (Battjes and Janssen, 1978; Thornton and Guza, 1982). These bore models provide robust estimates of bulk dissipation rates within the surf zone. However, the spectral characteristics of the energy losses are unknown, and somewhat arbitrary quasi-linear spectral forms of the dissipation function are used in Boussinesq models (Mase and Kirby, 1992; Eldeberky and Battjes, 1996).

Despite many studies on the shoaling evolution of wave frequency spectra, the evolution of directional wave spectra has not been thoroughly examined. The evolution of directional wave spectra is of great importance to the generation of longshore currents

and sediment transport, and the excitation of nearshore infragravity (0.005-0.05 Hz) motions. Laboratory and field experiments of directional wave spectra outside the surf zone show the expected refraction of incident waves and energy transfers to harmonic components with propagation directions that are in agreement with the theoretical triad interaction rules (Freilich et al., 1990; Elgar et al., 1993). Field observations of wave transformation across the surf zone show that wave breaking does not significantly alter mean propagation directions, but it significantly increases the directional spreading (Herbers et al., 1999). The mechanisms for this directional broadening are not currently understood.

This thesis presents a field validation test of a stochastic Boussinesq model (Herbers and Burton, 1997) for directionally spread waves propagating over an alongshore uniform beach. Norheim et al. (1998) tested a one-dimensional implementation of the model for nonbreaking, unidirectional waves with observations of wave frequency spectra evolution outside the surf zone on a natural beach. The predicted spectra were found to be in good agreement with both measured spectra and predictions of the deterministic Boussinesq model of Freilich and Guza (1984). A full two-dimensional implementation of the stochastic model for directionally spread waves was recently completed (Herbers et al., manuscript in preparation) including a parameterization of surf zone dissipation (Whitford, 1988).

The field data used for model validation were collected during the SandyDuck experiment conducted near Duck, North Carolina, during the fall of 1997 (Feddersen et al., 2000; Elgar et al., 2001). An extensive array consisting of 69 pressure gages, 33 electromagnetic current meters, and 33 downward-looking sonar altimeters to monitor the

sea bed level, was deployed in a 200 m (alongshore) by 420 m (cross-shore) area extending from about 1 to 5 m water depth. High quality data were collected during a four-month period spanning a wide range of conditions. Four alongshore pressure sensor arrays were selected from this experiment to estimate the evolution of the frequency-directional wave spectrum $E(f, \theta)$ across the beach. Additional estimates of $E(f, \theta)$ were extracted from the permanent pressure gage array maintained in 8m depth by the Army Corps of Engineers.

The model was initialized with $E(f, \theta)$ estimates in both 8m and 5m depth to examine the sensitivity of the model to initial conditions. Model predictions of $E(f, \theta)$ at the shallower arrays were compared with the observed spectra. The shoaling evolution of several important wave parameters will be examined to quantify the accuracy of the model. These parameters include the significant wave height, sea surface skewness and asymmetry, infragravity variance, mean propagation direction, and directional spread. Several case studies will be examined in detail to better understand model tendencies. The overall model performance will be examined using statistical analysis of predictions derived from the entire experiment.

A description of the field experiment and procedures for data reduction and analysis are given in chapter II. The model equations and implementation are briefly reviewed in chapter III. Several case studies with different wave conditions are examined in chapter IV. Results for the entire data set are presented in chapter V, followed by conclusions in chapter VI.

II. FIELD EXPERIMENT AND DATA ANALYSIS

The non-linear evolution of the frequency-directional wave spectrum $E(f, \theta)$ across a natural beach is examined using extensive measurements collected at the U.S. Army Corps of Engineer's Field Research Facility (FRF), Duck, NC, during the SandyDuck experiment in the summer/fall of 1997 (Elgar et al., 2001; Feddersen et al., 2000). This site is located on a straight barrier island with an 80 km wide, shallow (20-50 m depth) shelf that is fully exposed to the Atlantic Ocean. This study will focus on the densely instrumented nearshore region (210-900 m offshore) where the shallow water effects on the evolution of the $E(f, \theta)$ (nonlinear triad interactions, surf zone breaking) are most pronounced.

The bathymetry (figure 1) is characterized by a gently sloping inner shelf ($\sim 1:250$) and a slightly steeper beach ($\sim 1:100$). Bathymetric surveys of the nearshore region indicate that the beach topography changed slightly over the course of the experiment. The sand bar located approximately 300m offshore remained fairly stationary with a crest approximately 5 m below mean sea level. The beach morphology was more dynamic on the beach face shoreward of the nearshore arrays, but this region is not examined in this study.

A plan view of the beach with instrument locations is shown in figure 2. Directional wave data were available from a permanent array of pressure sensors located about 900 m from shore in 8 m depth, which is maintained by the FRF. This 15-element array has an aperture of 250 m alongshore and 120 m cross-shore, and is sampled at a 2 Hz rate that resolves waves with frequencies up to about 0.3 Hz. A subset of 9 sensors aligned in the alongshore direction was used here to estimate $E(f, \theta)$ (figure 2).

The extensive 2-dimensional nearshore array consisted of 69 pressure gauges (P) and 33 current meters (U,V). Four linear alongshore arrays of pressure sensors each with an aperture of 210 m were used to obtain estimates of $E(f,\theta)$. These arrays (labeled B, C, E, and F in figure 2) were positioned at offshore distances of 210, 260, 375, 500 m in nominal depths of 2.9, 3.7, 3.9, and 5.1 m, respectively (figure 2). The nearshore arrays also included downward-looking sonar altimeters (S) that provided continuous sea-bed level measurements. All nearshore instruments were connected to a central data collection center onshore. Data were collected nearly continuously with a sample rate of 2 Hz between 2 August and 3 December, 1997.

Alongshore homogeneity over the extent of the nearshore arrays was verified by intercomparing the measured spectra of each sensor in the array, as well as the coherence and phase spectra of redundant array lags. Elgar et al. (2001) noted that the southernmost cross-shore sensor transect of the array consistently recorded spectral density values lower than other array sensors for waves arriving from large, oblique southerly directions. These discrepancies are likely caused by the close proximity to the FRF research pier pilings creating partial wave blocking and a large scour hole (figure 1). Data from these sensors were excluded from the analysis.

In this study, frequency-directional wave spectra were estimated from five alongshore arrays of pressure sensors (figures 2,3). Cross-shore arrays were not used because cross-shore depth variations cause significant cross-shore variations in spectral levels, particularly in surf zone where strong dissipation causes large gradients in wave height. The 180 degree directional ambiguity of the linear arrays was resolved by neglecting weak reflection of waves from shore (Elgar et al., 1994). The data from the

arrays were archived in synchronized 3-hour data records. Only the first 102 minutes of each record were used here to estimate $E(f, \theta)$ in order to reduce nonstationary effects of tidal fluctuations in water depths.

Array cross-spectra were calculated based on Fourier transforms of overlapping 512 sec segments. Merging 3 frequency bands resulted in estimates with a frequency resolution of 0.0059 Hz and 72 degrees of freedom. At each frequency, f , the directional distribution of wave energy, $S(\theta; f)$, was estimated from the array cross-spectra using the variational technique described in Herbers and Guza (1990). The direction, θ , is defined relative to the local shoreline orientation with $\theta = 0$ corresponding to normal incidence to the beach (waves arriving from 70 true N), and θ is positive (negative) for waves approaching the beach from northerly (southerly) directions. The surface elevation frequency spectrum, $E(f)$, was obtained by averaging the measured auto-spectra and applying a linear theory depth correction. The $S(\theta; f)$ estimates were combined with $E(f)$ estimates to form the wave frequency-directional spectrum, $E(f, \theta) = E(f)S(\theta; f)$. Additionally, bispectra were calculated from the time series data to obtain estimates of the bulk wave skewness and asymmetry (e.g. Elgar and Guza, 1985).

Bottom profiles used in numerical model computations were estimated based on both the Coastal Research Amphibious Buggy (CRAB) beach surveys conducted by the FRF staff and the sonar altimeter data. CRAB high-spatial resolution surveys were conducted intermittently in time with gaps ranging from several days to a week. All depths were referenced to the NGVD datum. The cross-shore profile in the array vicinity measured by the CRAB was linearly interpolated over time to correspond to the spectral

wave data estimated at three-hour intervals. Since the CRAB surveys cover only the nearshore region out to about 5 m depth, the profiles were extended seaward to the 8 m array using a linear interpolation, assuming that the seabed level at the center of the 8 m array (-8.08 m) did not change during the course of the experiment. Tide corrections were applied to the beach profiles using a 102 minute sea level average obtained from the FRF tide gauge. The FRF tide gauge did not operate during the periods 10/21/97 19:00 EST – 10/22/97 16:00 EST and 11/23/97 19:00 EST – 11/25/97 16:00 EST. The 8 m array pressure sensor data was used to fill in the missing tide corrections.

The sonar altimeters recorded sea-bed level data nearly continuously in time (same sampling scheme as the pressure sensor data). Only 18 three-hour records were missing in the altimeter data during the entire experiment. However, the cross-shore resolution was poor with bed-level measurements at only 8 cross-shore positions (see figure 4). At each cross-shore position, only the working sonar altimeter located nearest the central axis of the arrays (alongshore coordinate 830 m) was used in the analysis. Sonar altimeter-based depth profiles were interpolated both spatially and temporally (to cover gaps in the data collection) and tide corrected. A linear interpolation was used in space and time, with the exception of the spatial interpolation across the bar region where a cubic spline interpolation was employed to better represent the sand bar crest (figure 5a, 5b).

The root-mean-square (RMS) error between beach profiles estimated from the CRAB and altimeter data are shown in figure 6b. The RMS difference between the two nearshore profile data sets is generally small (0.04 – 0.08 m), with the exception of a few periods (notably 15-23 October and 6-9 and 13-15 November) with more energetic waves

when the RMS differences were as large as 0.16 m (figures 6a and 6b). In these storm events when the CRAB could not safely take measurements, systematic differences between the CRAB and altimeter depth estimates suggest significant erosion close to shore. In the present study, the CRAB surveys were used in low-moderate wave conditions ($H_s < 2$ m) when sea bed levels did not vary significantly between surveys. Profiles based on the sonar altimeter data were used during two wave events (10/18/97 0100 – 10/20/97 2200; 11/01/97 0100 – 1000) when significant wave heights exceeded 2 m and the bottom morphology was more dynamic.

THIS PAGE INTENTIONALLY LEFT BLANK

III. MODEL DESCRIPTION AND IMPLEMENTATION

The nonlinear, spectral wave shoaling model used in this study is a stochastic Boussinesq model for directionally spread waves shoaling on a gently sloping beach with straight and parallel depth contours (Herbers and Burton, 1997; Herbers et al., manuscript in preparation). The model is based on a third-order closure scheme and consists of a coupled set of first-order evolution equations for the wave spectrum $E(\omega, l)$ and bispectrum $B(\omega_1, l_1, \omega_2, l_2)$

$$\begin{aligned} \frac{dE(\omega, l)}{dx} = & \left\{ -\frac{1}{2h} \frac{dh}{dx} - D_1(\omega, l) \right\} E(\omega, l) \\ & + \frac{3\omega}{2h^{3/2} g^{1/2}} \int_{-\infty}^{\infty} d\omega' \int_{-\infty}^{\infty} dl' \text{IM} \{ B(\omega', l', \omega - \omega', l - l') \} \end{aligned} \quad (3.1)$$

$$\begin{aligned} \frac{dB(\omega', l', \omega - \omega', l - l')}{dx} = & \left\{ -\frac{3}{4h} \frac{dh}{dx} - (1+R)D_2(\omega', l', \omega - \omega', l - l') - i \left[\frac{h^{1/2} \omega' (\omega - \omega') \omega}{2g^{3/2}} + \frac{(gh)^{1/2} (\omega l' - \omega' l)^2}{2\omega' (\omega - \omega') \omega} \right] \right\} B(\omega', l', \omega - \omega', l - l') \\ & - i \frac{3}{2h^{3/2} g^{1/2}} [\omega' E(\omega - \omega', l - l') E(\omega, l) + (\omega - \omega') E(\omega', l') E(\omega, l) - \omega E(\omega', l') E(\omega - \omega', l - l')] \end{aligned} \quad (3.2)$$

where ω is frequency, l is alongshore wavenumber, h is water depth, g is gravity, and $\text{IM} \{ \}$ is the imaginary part. The two-dimensional spectrum $E(\omega, l)$ describes the surface elevation spectral density of component (ω, l) , and the four-dimensional (complex) bispectrum $B(\omega_1, l_1, \omega_2, l_2)$ defines the phase relationship of a triad consisting of components (ω_1, l_1) , (ω_2, l_2) , and $(-\omega_1 - \omega_2, -l_1 - l_2)$. A heuristic parameterization of wave breaking effects was included in equations 3.1 and 3.2 to extend the model into the surf zone. The damping terms, D_1 and D_2 are expressed in terms of a frequency-dependent dissipation function $G(\omega)$.

$$D_1(\omega, l) = G(\omega) + G(-\omega) \quad (3.3)$$

$$D_2(\omega', l', \omega - \omega', l - l') = G(\omega') + G(\omega - \omega') + G(-\omega) \quad (3.4)$$

Following Mase and Kirby (1992) and Chen et al. (1997) a quadratic frequency dependence was included in the model

$$G(\omega, l) \propto \omega^2 \quad (3.5)$$

The bulk dissipation rate, $\varepsilon = 2\rho g^{3/2} h^{1/2} \int_{-\infty}^{\infty} G(\omega) d\omega$, was estimated using a parameterization given by Whitford (1988)

$$\frac{3\sqrt{\pi}}{16h} \rho g b \bar{f} H_{ms}^3 \left\{ 1 + \tanh \left[8 \left(\frac{H_{ms}}{\gamma h} - 1 \right) \right] \right\} \left\{ 1 - \left[1 + \left(\frac{H_{ms}}{\gamma h} \right)^2 \right]^{-5/2} \right\} \quad (3.6)$$

where \bar{f} is the mean frequency, H_{ms} is the root mean square wave height and γ , b are adjustable coefficients. Additionally, a relaxation term with an adjustable coefficient R is introduced in the bispectrum equation to provide a rerandomization of phases in the wave breaking process.

The adjustable breaking parameters were calibrated using extensive observations of the evolution of wave frequency spectra across a barred beach (neglecting directional effects), and fixed at values: $\gamma = (0.30)$, $b = (0.25)$, and $R = (2.5)$ (Herbers et.al; manuscript in preparation).

The model is initialized at the offshore boundary with an observed frequency-directional spectrum $E(f, \theta)$ that is transformed to (ω, l) space. The initial bispectrum is estimated with second order, finite depth theory (Hasselmann et al., 1963). To examine the sensitivity to offshore boundary conditions, the model was initialized at both the 8 m and F arrays.

Equations 3.1 and 3.2 were integrated using a fourth order Runge Kutta scheme with a fixed step size of 0.25 m from the offshore boundary to the B array. The model was implemented with 54 frequencies (spanning the full range 0.00585 – 0.3164 Hz of the observed spectra), and 85 alongshore wavenumbers. To prevent instability of the model, the alongshore wavenumber was restricted (maximum k values of ± 0.19 rad/m). As a result of this truncation, high frequency waves entering the model domain at large oblique angles are excluded.

The frequency-directional spectra predicted at all shoreward arrays are compared to observed spectra in chapter 4. To quantify the model performance, various important bulk parameters: the significant wave height (H_s), skewness and asymmetry (e.g. Elgar and Guza, 1995), infragravity variance (in the frequency range 0.00585 – 0.0468 Hz), and the mean direction ($\bar{\theta}$) and directional spread (σ_θ) (e.g. Herbers et al., 1999), were extracted from the predicted spectra and bispectra, and are compared to observed values in chapters 4 and 5.

THIS PAGE INTENTIONALLY LEFT BLANK

IV. CASE STUDIES

Four case studies spanning a wide range of wave conditions were selected to illustrate in detail the model's characteristics. In each case, results are presented for model runs initialized in both 8m and 5m (F-Array) depths. Case I (August 7, 1997 01:00 EST) is characterized by a broad spectrum of small, non-breaking waves. Case II (August 10, 1997 04:00 EST) features the evolution of a low energy, narrow swell spectrum again with little or no breaking. In case III (September 12, 1997 07:00 EST) more energetic swell was observed with waves breaking across the inner part of the nearshore array transect. Finally in case IV (October 19, 1997 16:00 EST), collected during a severe Noreaster storm that produced the largest waves of the entire data set, the entire instrumented transect was within the surf zone. For each case study, the frequency spectrum $E(f)$, and frequency-directional spectrum $E(f, \theta)$ predicted at each of the arrays are compared to the observed spectra (figures 7, 10, 13, 16; only model runs initialized at the F array are shown). The predicted and observed cross-shore evolution of the significant wave height H_s , sea surface asymmetry and skewness, infragravity variance, mean direction $\bar{\theta}$, and directional spread σ_θ are compared in figures 8, 9, 11, 12, 14, 15, 17, and 18. The significant wave height $\left(H_s = 4\sqrt{\iint E(f, \theta) df d\theta}\right)$ represents the average height of the highest 1/3 waves. Skewness and asymmetry characterize the nonlinearity of the waves. The asymmetry describes the pitched forward (positive) or backward (negative) profile of the wave, while the skewness describes the peakedness of the wave (see Elgar and Guza, 1985 for definitions). The infragravity variance is the variance within the infragravity frequency range (0.0059 – 0.0468 Hz) that contains low

frequency waves excited by nonlinear interactions of the incident waves in shallow water. The mean direction and directional spread are energy weighted bulk average values over the spectrum (see Herbers et al., 1999 for definitions).

CASE I: AUGUST 7, 1997 01:00 EST

The small incident waves ($H_s = 0.52\text{m}$) are characterized by a bimodal spectrum that consists of a southeast swell (0.13 Hz) and a northeasterly swell (0.2 Hz). The predicted frequency-directional spectra show virtually no evolution across the transect, in good agreement with the observed spectra (figure 7).

The significant wave heights are accurately predicted in the F array-initialized model run, whereas the 8m-initialized run overpredicts H_s by about 10% at the nearshore arrays, probably because the high frequency incident waves violate the shallow water approximation of the Boussinesq model (figure 8). Predicted sea surface asymmetry and skewness values are small (<0.1) at all arrays, consistent with the observed values (figure 8).

The observed amplification of infragravity variance near the shore (about a factor of three between the 8m and B arrays) is predicted well by both model runs (figure 9). The 8m-initialized model run is slightly more accurate than the F array model run, but both model runs underpredict the sharp increase at the B array, possibly because reflection from shore is neglected in the model. The observed and predicted mean directions are close to normal incidence due to averaging over 2 swell systems arriving from opposite quadrants (figure 9). Both model runs reproduce the slight decrease in directional spread towards the shore caused by refraction (figure 9).

CASE II: AUGUST 10, 1997 04:00 EST

This day was characterized by moderate size non-breaking waves ($H_s = 0.87$ m offshore increasing to 0.97 m inshore) arriving at near normal incidence ($\bar{\theta} = -10$ deg). The frequency spectrum is narrow with a peak frequency $f_p = 0.09$ Hz (figure 10). Strong nonlinear energy transfers are evident in the dramatic growth of harmonic peaks at frequencies $2f_p = 0.18$ Hz and $3f_p = 0.27$ Hz between the F and C arrays. The predicted harmonic spectral levels and directions (aligned with the dominant swell) are in good agreement with the observations (figure 10). Interestingly, both the observed and predicted spectra show a decay of the second harmonic peak between the C and B arrays.

Both model runs indicate a slight overshooting of significant wave heights (figure 11). The errors are larger for the 8m-initialized model run (about 10% at array B) than for the F array-initialized model run (7%), suggesting the errors are caused by inaccuracies of the shallow water approximation used in the Boussinesq equations. Asymmetry is predicted well by both model runs (figure 11), showing a positive maximum of 0.3 (pitched forward wave crests) seaward of the bar and a negative maximum of -0.2 (pitched backward crests) inshore of the bar. The observed and predicted negative asymmetry indicates that the observed decay of the second harmonic peak inshore of the bar is the result of a reversal of nonlinear energy transfers (Norheim et al., 1998). Both model runs overpredicted skewness by about 25%, but reproduce qualitatively the increase to a maximum value of about 1 over the bar followed by a decrease towards the shore (figure 11).

Again, the infragravity variance increases in the observations as well as the models (figure 12). As in case I, the 8m model run predicts more accurately the amplification of infragravity waves near the shore, but both model runs underpredict the

amplification of infragravity waves at the B array. The predicted shifting of $\bar{\theta}$ from -10 deg at the 8m array to -5 deg at the B array is in good agreement with the observed directions (figure 12). However, whereas the model predicts a decrease of σ_{θ} from 15 deg to 10 deg, the observed σ_{θ} are nearly uniform across the instrument transect.

CASE III: SEPTEMBER 12, 1997 07:00 EST

The incident waves on this day are characterized by a similar narrow swell spectrum ($f_p = 0.08$ Hz, $\bar{\theta} = -10$ deg), but are more energetic than in case II. The significant wave height H_s decreases from a maximum value of 1.4 m offshore of the bar to 1.2 m inshore of the bar (figure 14), indicating breaking of the larger waves on the bar. The growth of the harmonic peaks through nonlinear wave-wave interactions is again evident in the spectra, and the spectral levels and direction (aligned with the dominant swell direction) are well predicted by the model.

As in the earlier cases, the model tends to overshoot the waves, producing maximum wave heights at the E array that are slightly larger than observed. The errors are again larger for the model run initialized at the 8m array (8%) than for the run initialized at the F-array (5%), suggesting the errors result from inaccuracies in the shallow water approximation. The decrease of the significant wave height inshore of the E array is accurately predicted by both model runs (figure 14). Predicted asymmetry increases to a maximum positive value of 0.4 on the bar (associated with energy transfers to high frequency harmonics) followed by a decrease to small negative values inshore of the bar (figure 14). The skewness predictions show two maxima (values about 1 at cross-shore distances of 250 and 410 m) with slightly smaller values (0.8) on the bar (figure 14). Predicted skewness and asymmetry variations in both model runs are in good agreement with the observations.

The amplification of infragravity waves near the shore is predicted accurately by the model run initialized in 8m depth, whereas the run initialized at the F array underpredicts the infragravity variance by about 30% (figure 15). A possible explanation for this large discrepancy is inaccuracy of the initial bispectrum that is based on a local horizontal bottom solution of second order wave theory (Herbers and Burton, 1997). Both model runs overpredict changes in $\bar{\theta}$ toward normal incidence by 3-5 degrees and overpredict the directional narrowing of the spectrum. The observed σ_θ values at the B array are about 30% larger than the predicted values, suggesting that wave breaking causes a directional broadening that is not represented in the model.

CASE IV: OCTOBER 19, 1997 16:00 EST

In this case with the largest waves of the entire data set, the entire instrument transect was in the surf zone. The observed and predicted frequency-directional spectra again show development of harmonic peaks aligned with the dominant 0.10 Hz swell. However, at the inshore C and B arrays predicted nonlinear interactions have filled in the valleys between the harmonic peaks, producing a broad, featureless spectrum, in good agreement with the observed frequency spectra (figure 16).

The significant wave height decreases from 3.5 m at the 8m array to 1.5 m at the B array (figure 17). The wave height decay is predicted well by both model runs (figure 17). The 8m-initialized model run initially predicts too much dissipation (underpredicting H_s by 25% at the F array), but yields accurate H_s predictions at the inshore arrays (figure 17). The asymmetry and skewness are predicted well by both model runs (figure 17). In contrast to nonbreaking case II, the observed and predicted asymmetry values are positive over the entire transect, indicating that no reversal in energy transfers to lower frequencies occurred in this case. Both model runs predict a

maximum asymmetry value at about 0.4 near the E array decreasing to near-zero values at the B array, in good agreement with the observations (figure 17). Both model runs show nearly uniform (about +0.5) skewness values throughout the transect that are slightly (10-20%) smaller than the observed values (figure 17).

The evolution of the infragravity variance is predicted well by both model runs (figure 18). The observed and predicted cross-shore variations are weak compared to the previous cases. The infragravity variance decreases near the shore, possibly due to some dissipation (figure 18). The predicted turning of $\bar{\theta}$ toward normal incidence (from +10 deg in 8m depth to +4 deg at the B array) owing to refraction is in good agreement with the observed directions (figure 18). Whereas the predicted σ_θ decreases from 18 degrees in 8m depth to 15 degrees at the B array, the observed σ_θ increase slightly to a maximum value of 22 degrees at the B array (figure 18). These results suggest that wave breaking causes a significant directional broadening of wave spectra in the surf zone.

V. OVERALL MODEL PERFORMANCE

The overall performance of the model for the entire data set is examined here with scatterplots of predicted versus observed significant wave heights (figure 19), infragravity variance (figure 20), skewness and asymmetry (figure 21), and mean direction and directional spread (figure 22).

First, all 987 data runs were examined for bad data. The entire data run was discarded if the initialization spectrum from either the 8m or F arrays was missing or bad data. A total of 54 data runs were discarded. If data were missing or bad at any one of the shoreward E, C, or B arrays, the observed spectrum for that array was discarded. A total of 41 spectra were discarded. After bad data were removed, scatterplots were created for each array located shoreward of the array used to initialize the model. In each scatterplot, a best fit line obtained through linear regression analysis is indicated (dashed diagonal line) as well as the one-to-one correspondence line (solid diagonal line). Results are shown only for model runs initialized at the F array that yielded the best overall wave height predictions (discussed below), with the exception of infragravity variances for which both 8m and F array initialized results are shown in figure 20.

Significant wave height scatterplots (figure 19) show generally good agreement for the entire data set, results for both the absolute H_s and H_s normalized by the initial H_s are shown. However, the model tends to underpredict H_s (by as much as 10%) when the observed H_s is greater than 1.5 m, suggesting a deficiency of the dissipation parameterization in high energy conditions. The normalized scatterplots show a tendency of a slight overprediction of H_s for nonbreaking waves (normalized $H_s \geq 1$) and a slight underprediction of H_s within the surf zone (normalized $H_s \leq 1$) (figure 19).

Comparisons of observed and predicted (figure 20, both normalized by the initial values) infragravity variance show large discrepancies at the arrays located farther offshore, but improved correlation as the model progresses shoreward. These results suggest the main source of errors is the initialization of the bispectrum that is based on second-order wave theory for a horizontal sea bed. The model run initialized at the 8m array yields more accurate predictions of the infragravity variance at all shoreward arrays than the model run initialized at the F array, consistent with smaller bottom slope effects in deeper water.

The skewness predictions are well correlated with the observations for the entire data set, with slightly more scatter at the B array than at the other two arrays (figure 21). However, deviations of the best fit line from a one-to-one correspondence show a consistent 10-15% overprediction of skewness at all array locations. Skewness (observed and predicted) are positive at all arrays indicating that waves always have peaked crest profiles in the nearshore region. The asymmetry predictions are also in good agreement with observations. The asymmetry comparisons show slightly more scatter than the skewness comparisons, but virtually no bias. Only at the shallower B array, asymmetry predictions are biased low for large asymmetry values. Asymmetry is consistently positive at the E array, but negative values are observed and predicted at C and B arrays (figure 21) that are indicative of reversals of energy transfers to the spectral peak inshore of the sand bar.

Mean direction predictions are well correlated with the observations at all array locations (figure 22). The predicted angles are on average slightly closer to normal incidence, possibly because high-frequency waves traveling at large oblique angles are

excluded in the initial model spectra. Wave refraction is evident in the smaller range of observed and predicted $\bar{\theta}$ at shallow inshore array locations. The directional spread σ_θ is consistently underpredicted at all locations (figure 22). This bias, increasing from roughly 10% at array E to 25% at array B, is likely caused by the exclusion of high-frequency, high angle waves in the model and surf zone scattering effects not represented in the model.

To summarize the accuracy of the model, errors in the model predictions are quantified with a mean bias, RMS error, and scatter index (SI), defined as

$$bias = \frac{1}{N} \sum_{i=1}^N y_i - x_i \quad (5.1)$$

$$RMS \text{ error} = \sqrt{\frac{1}{N} \sum_{i=1}^N (y_i - x_i)^2} \quad (5.2)$$

$$SI = \frac{RMS \text{ error}}{\sqrt{\frac{1}{N} \sum_{i=1}^N x_i^2}} \quad (5.3)$$

where y is predicted, x is observed, and N is the number of observations. These error statistics were calculated for significant wave height, asymmetry, skewness, infragravity variance, mean direction, and directional spread, based on predictions at all arrays shoreward of the array used to initialize the model. The results together with a correlation coefficient, are listed in tables 1 (model initialized at the 8m array) and 2 (model initialized at the F array).

The F array initialized model runs yielded consistently more accurate significant wave heights than the 8m array initialized model runs. This can be deduced from the higher correlation coefficient (0.991 for F, 0.986 for 8m) and the lower bias (0.021 m for F, 0.047 m for 8m), RMS error (0.055 m for F, 0.081 for 8m), and SI (0.063 for F array, 0.092 for 8m). Possible explanations for these differences include inaccuracies in the shallow water approximation that affect model results in deeper water and a breakdown of the dissipation parameterization in large wave conditions.

Larger errors are observed in sea surface skewness and asymmetry predictions, but no significant differences are noted between model runs initialized at the 8m and F arrays.

Infragravity variance is predicted more accurately by the model run initialized in 8m depth than the model run initialized at the F array as noted in the smaller negative bias (-0.00018 m^2 for 8m, -0.00034 m^2 for F), RMS error (0.00056 m^2 for 8m, 0.00070 m^2 for F), and SI (0.19 for 8m, 0.21 for F). These differences are likely caused by errors in the initialization of the bispectrum.

Mean direction predictions of model runs initialized at the F array are more accurate than those initialized in 8m depth as exemplified by its higher correlation coefficient (0.972 for F, 0.915 for 8m), and the lower RMS error (3.8 deg for F, 5.9 for 8m) and SI (0.28 for F, 0.40 for 8m). Note that the bias is small owing to cancellation of a negative bias for negative (southerly) angles and a positive bias for positive (northerly) directions (figure 22).

There is not much difference between the error statistics of 8m-initialized and F array-initialized model predictions of σ_θ . The bias is slightly smaller for the F array-

initialized model runs, but in both cases low correlation coefficients (0.792 and 0.807) are observed, suggesting an important physical mechanism is missing in the model. Whereas the skewness predictions show smaller SI (0.34-0.37) and higher correlation coefficients (0.947-0.949) than the asymmetry predictions (0.42-0.45, 0.903-0.905), the asymmetry predictions have smaller bias. An important source of errors for both skewness and asymmetry predictions is the parameterization of wave breaking. Earlier studies (Chen et al., 1997) using a deterministic Boussinesq model show comparable agreement of skewness and asymmetry predictions with field and lab data and also indicate a strong sensitivity to the choice of dissipation function.

THIS PAGE INTENTIONALLY LEFT BLANK

VI. SUMMARY

A stochastic, nonlinear wave shoaling model based on Boussinesq equations and a third-order, weakly non-Gaussian closure scheme (Herbers and Burton, 1997) was validated using a comprehensive field data set. The model predicts the evolution of directionally spread waves propagating over an alongshore uniform beach. The model consists of a coupled set of evolution equations for the wave spectrum and bispectrum that incorporates linear shoaling and refraction effects and nonlinear energy exchanges in near-resonant triad interactions. Dissipation due to breaking is approximated using a frequency dependant empirical quasi-linear damping function and a relaxation to Gaussian statistics. The bulk dissipation rate is based on a bore model (Thornton and Guza, 1983; Whitford, 1988). The model was verified with field data from five alongshore arrays deployed at the U.S. Army Engineer Field Research Facility, Duck, North Carolina from August to December 1997 as part of the SandyDuck experiment. Estimates of frequency-directional spectra were obtained from all 5 arrays at 3 hour intervals for the entire experiment. Accurate depth profiles were obtained from frequent surveys and continuous sea bed level measurements at the array locations. Model runs are presented initialized in both 8m or 5m depths to examine the sensitivity of the model to initial conditions.

The shoaling evolution of the frequency-directional spectra was examined in detail for four case studies including nonbreaking and breaking waves. Predictions of important bulk parameters, significant wave height, sea surface asymmetry and skewness, infragravity variance, mean direction, and directional spreading, are compared with observed values for the entire experiment.

Predicted frequency-directional wave spectra reproduced accurately the observed development of harmonic peaks aligned with the dominant wave direction. However, the evolution inside the surf zone indicates that the observed spectra are directionally broader than the predicted spectra.

Significant wave height predictions are in good agreement with observations. The scatter index is 0.092 for model runs initialized in 8m depth and 0.063 for model runs initialized in 5m depth. The comparisons show a systematic model tendency to slightly overshoot the waves outside the surf zone (particularly for model runs initialized at the deeper 8m array) (tables 1,2). The model also tends to slightly over dissipate the waves inside the surf zone.

Infragravity waves are low frequency waves (nominally 0.005-0.05 Hz) that are believed to be important to sand bar formation and beach erosion. The observed dramatic infragravity wave growth in shallow water is reasonably well predicted by the model except near the shoreline where the model is biased low, possibly owing to neglected reflection. Model runs initialized in 8m depth are consistently more accurate than those initialized in 5m depth, indicating a sensitivity to the initial conditions that are based on second-order wave theory for a horizontal sea bed

Sea surface skewness and asymmetry are reasonably well predicted by the model, but the scatter index values are notably higher than for the wave height predictions (skewness 0.37-0.37; asymmetry 0.43-0.45) (tables 1,2). Both observed and predicted skewness are consistently positive and the model is biased high. The observed and predicted asymmetry are positive (pitched forward wave crests) at the offshore measurement locations. Negative asymmetry values (pitched backward wave crests) are

often observed and predicted inshore of the sand bar indicating reversal of nonlinear energy transfers from harmonics back to the dominant waves.

Although the stochastic Boussinesq wave model generally performed well, further model validation is needed on different beaches. Further possible extensions and refinements of the model include allowing for alongshore depth variations and reflection of low frequency waves from the shore. As faster computers with more memory become available in the future, this efficient spectral model may become a useful tool for real time surf forecasts.

THIS PAGE INTENTIONALLY LEFT BLANK

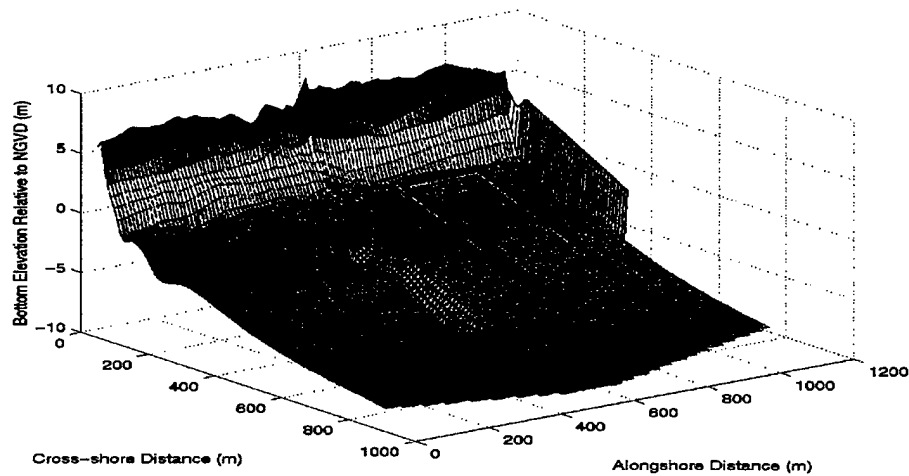


Figure 1. Bathymetry at the field site surveyed on September 16, 1997. The instrumented region is indicated with a red box. The trench located to the south of the instrumented region is caused by the presence of a 600m-long pier.

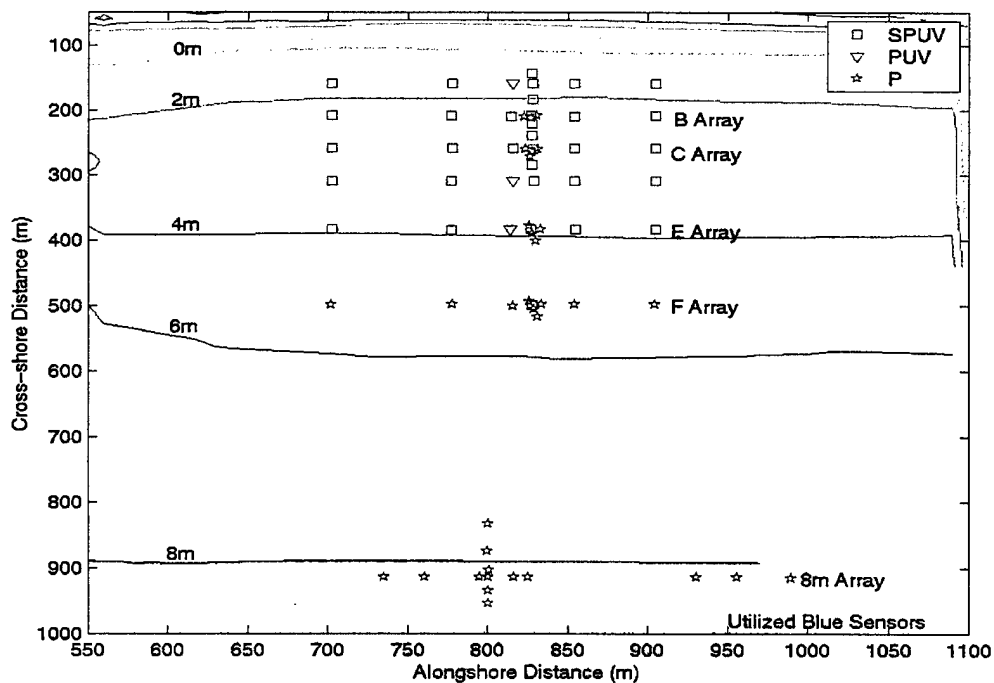


Figure 2. Plan View of Arrays. Instrument types include SPUV (collocated sonar, pressure sensor, and current meter), PUV (collocated pressure sensor and current meter) and P (pressure sensor). In this study 5 alongshore arrays of pressure sensors (labeled B, C, E, F, and 8m arrays, sensors indicated in blue) are used

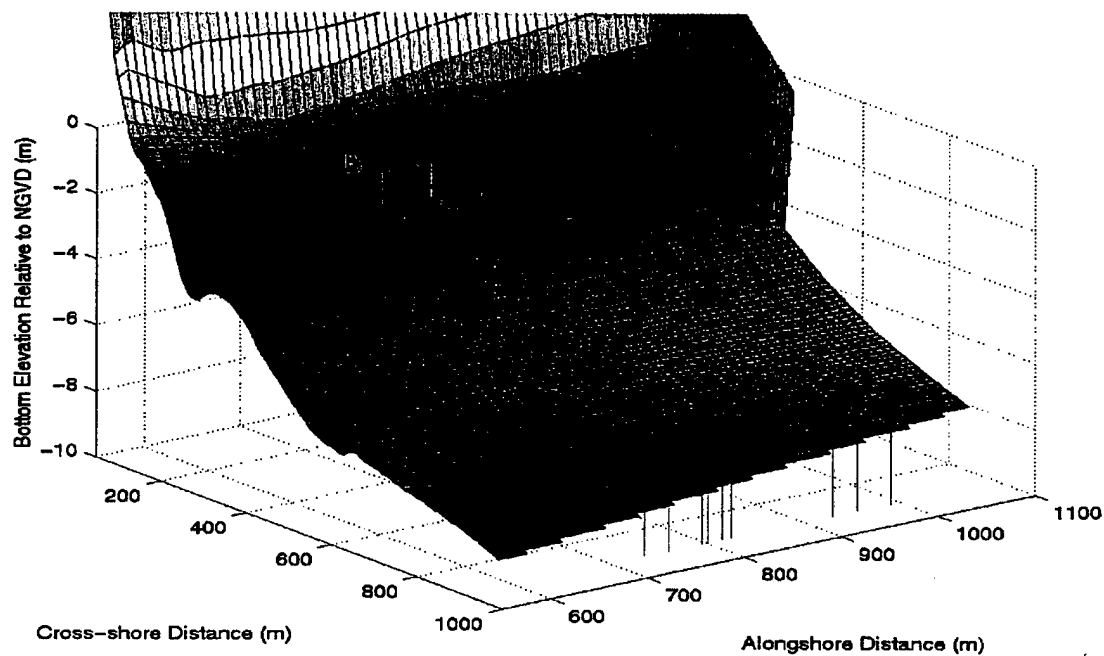


Figure 3. Three-dimensional view of pressure sensor arrays used in this study.

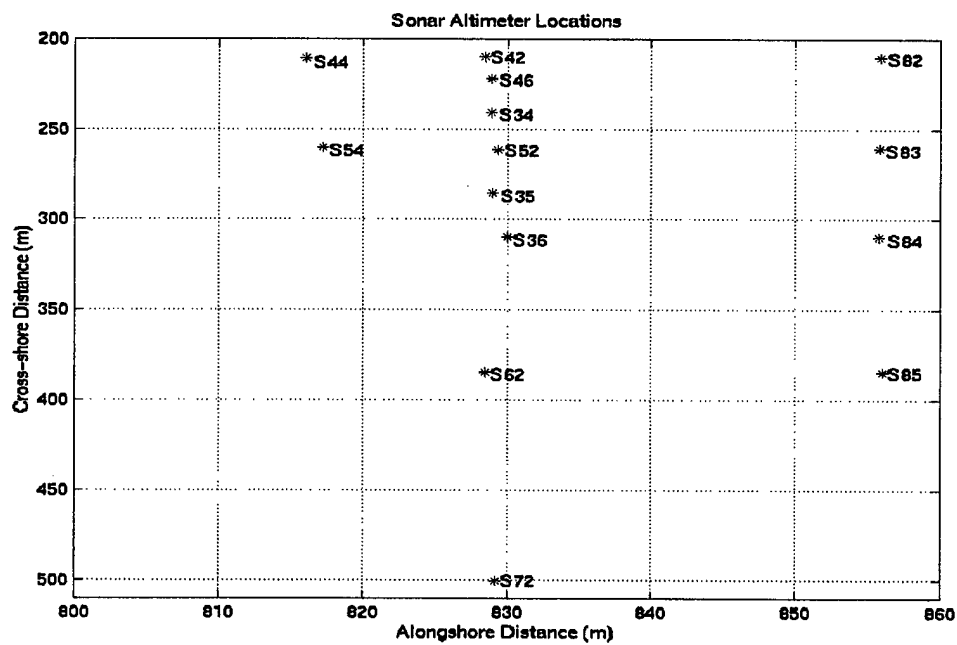


Figure 4. Sonar Altimeter Locations.

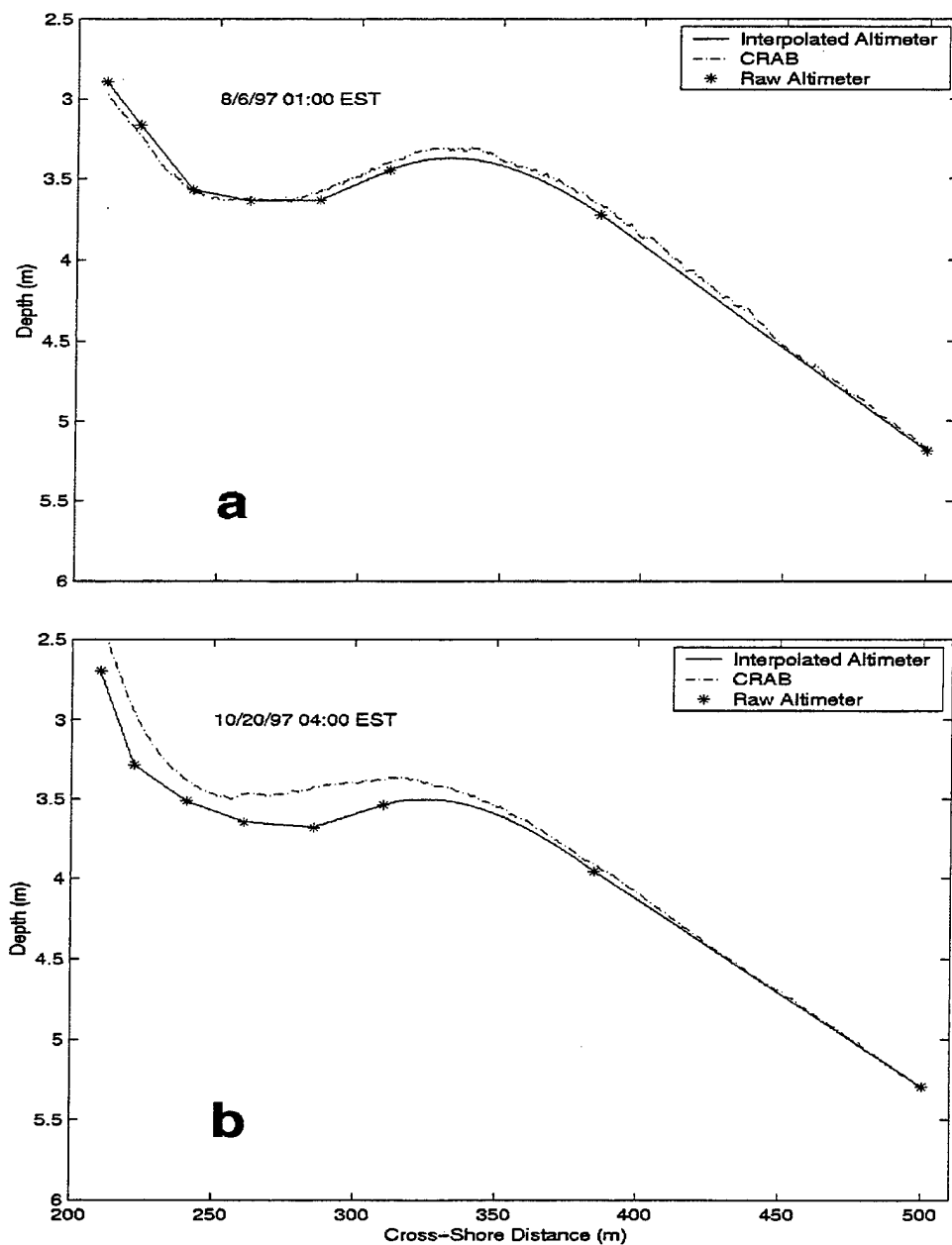


Figure 5. Comparison of beach profiles obtained from CRAB and sonar altimeter data. The sonar measurements (asterisks) were interpolated linearly, except over the sand bar where a cubic spline was used. (a) small wave conditions. (b) storm conditions.

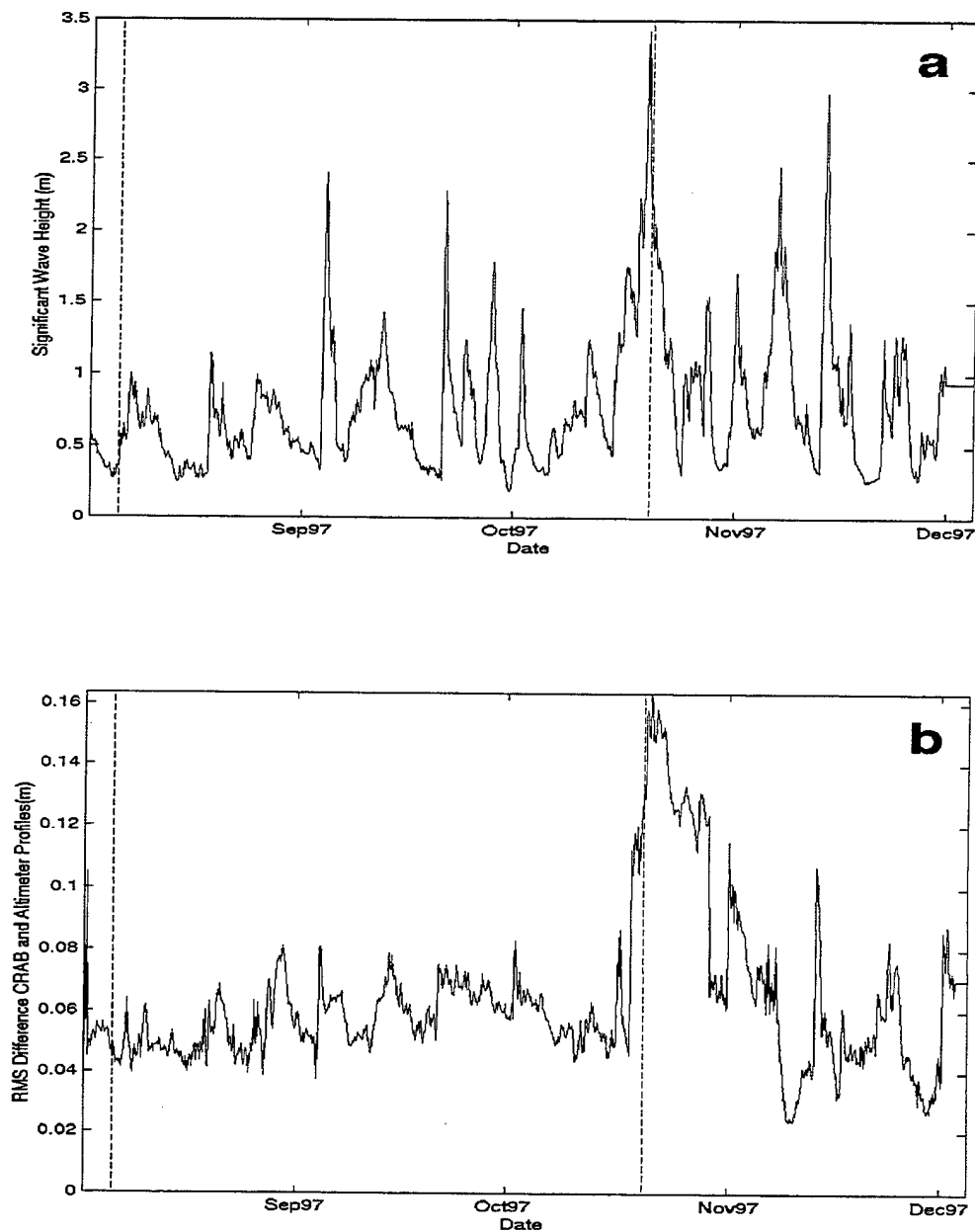


Figure 6. (a) Evolution of offshore H_s (measured in 8m depth) during the four month deployment. (b) Root-mean-square difference between beach profile based on CRAB and sonar altimeter data. Vertical dashed lines indicate times of beach profiles shown in figure 5.

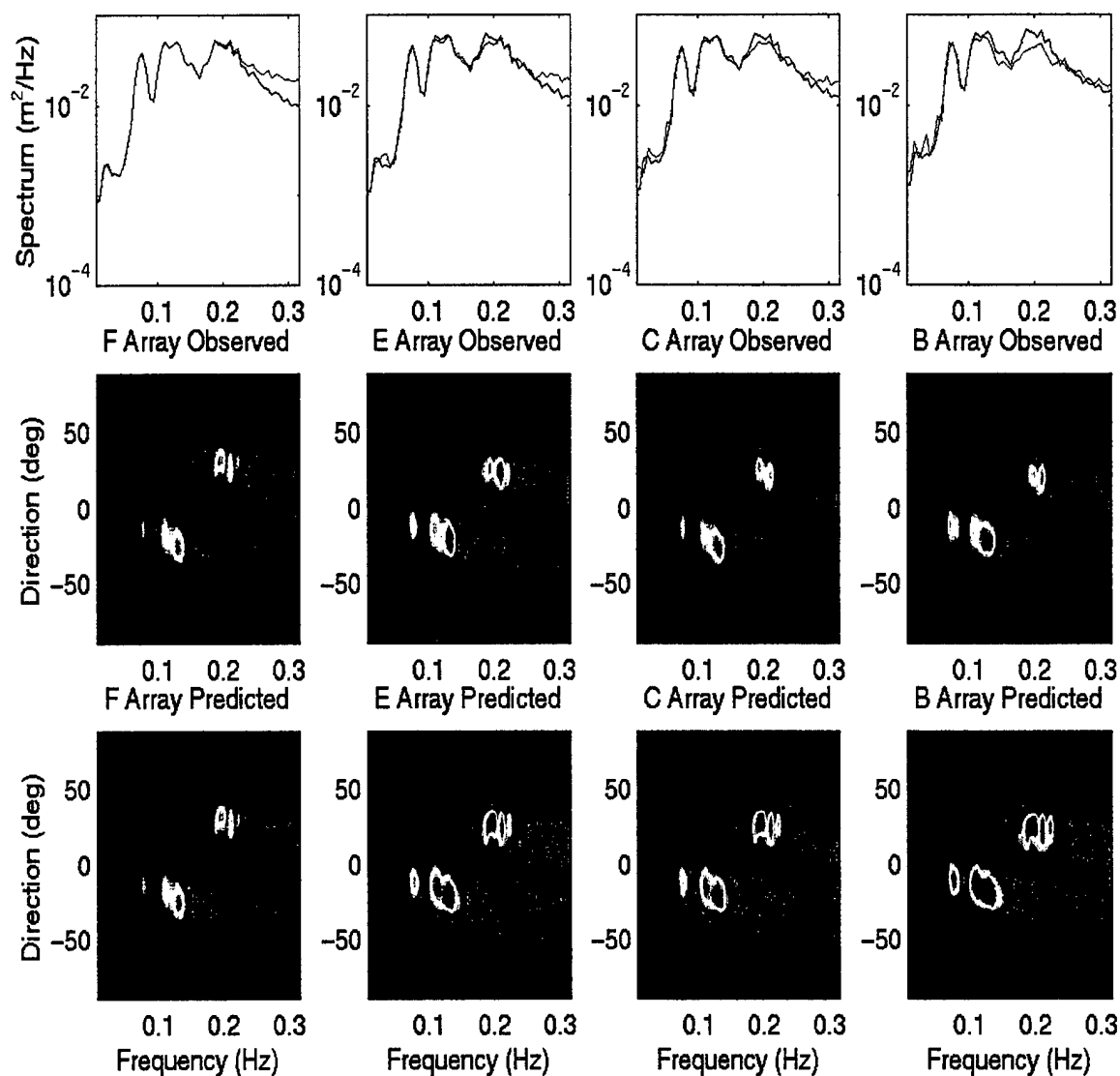


Figure 7. Frequency and frequency-directional spectra for Case I, (August 7, 1997 01:00 EST). The top panels display the (direction-integrated) frequency spectra at each array (blue line is model prediction, red line is observed spectrum at that array). The middle and lower panels contain the observed and predicted frequency-directional spectra, respectively. Note the exclusion of high frequency, large angle waves from the initializing model spectrum at the F array.

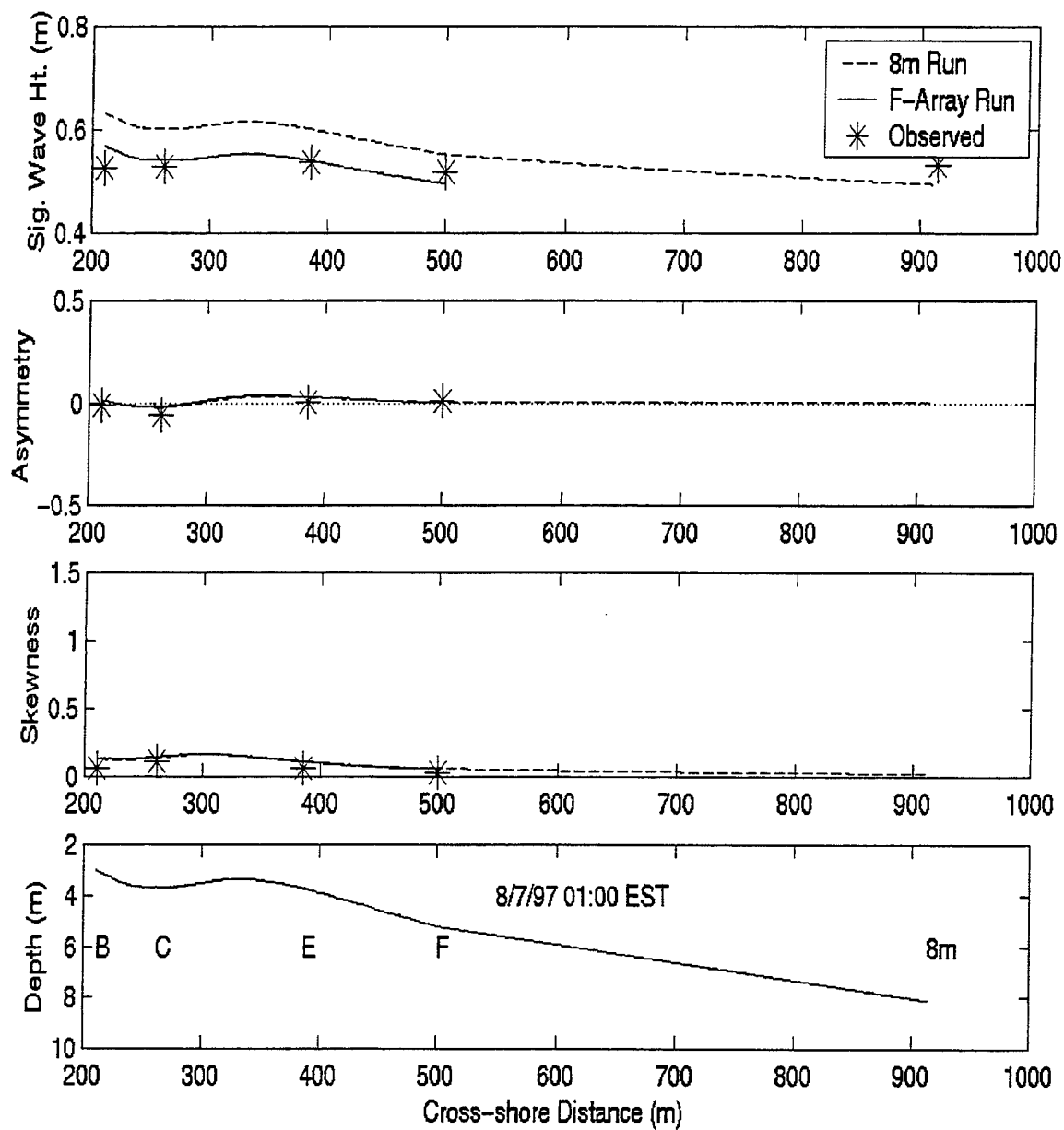


Figure 8. Case I, cross-shore shoaling evolution of significant wave height H_s , asymmetry, and skewness. Predictions of model runs initialized in 8m (dashed) and 5m (solid) depths are compared to observations (*) at each array. The depth profile and array locations are shown in bottom panel.

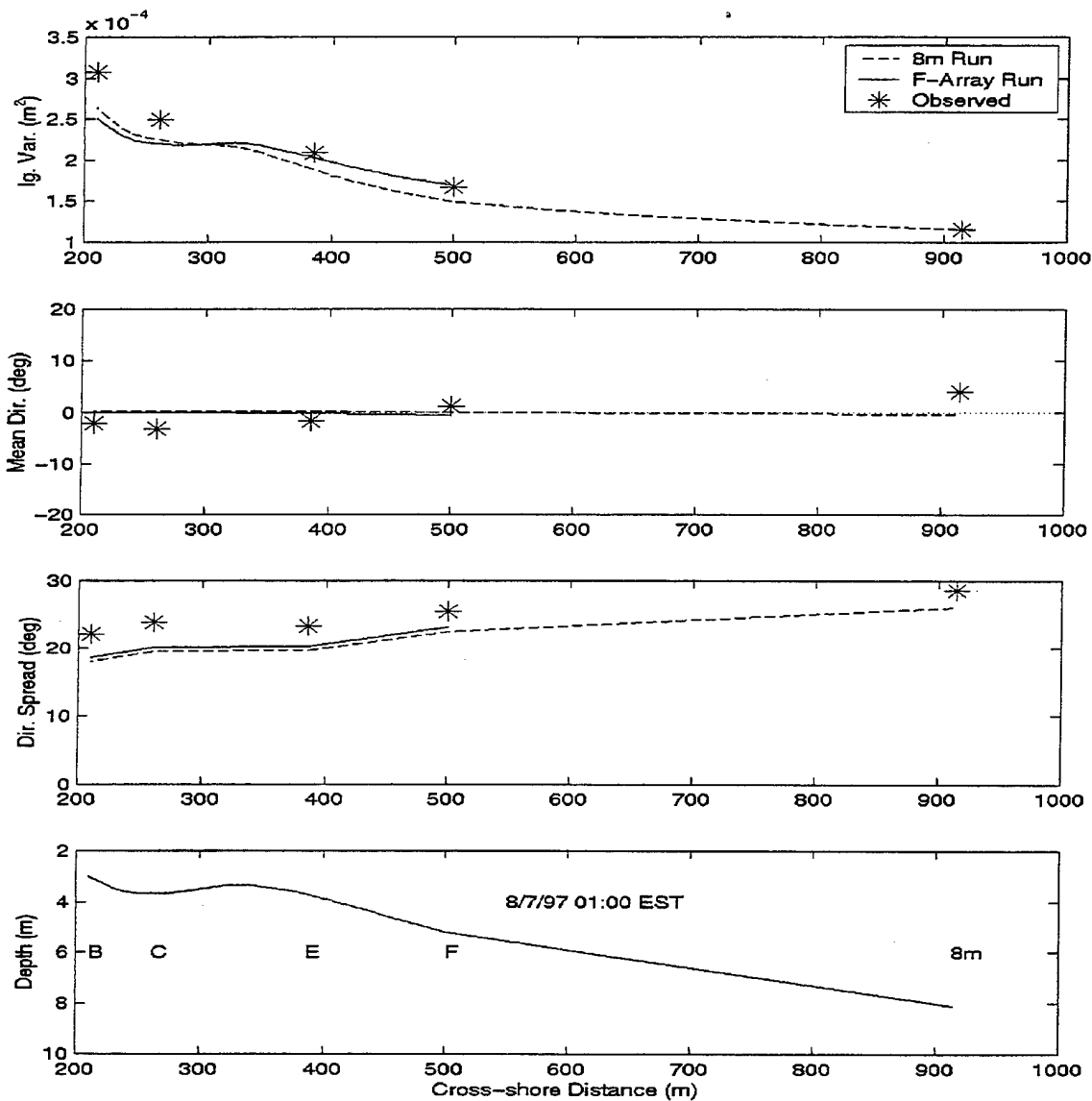


Figure 9. Case I, cross-shore shoaling evolution of infragravity variance, mean direction, and directional spread. Predictions of model runs initialized in 8m (dashed) and 5m (solid) depths are compared to observations (*) at each array. The depth profile and array locations are shown in bottom panel.

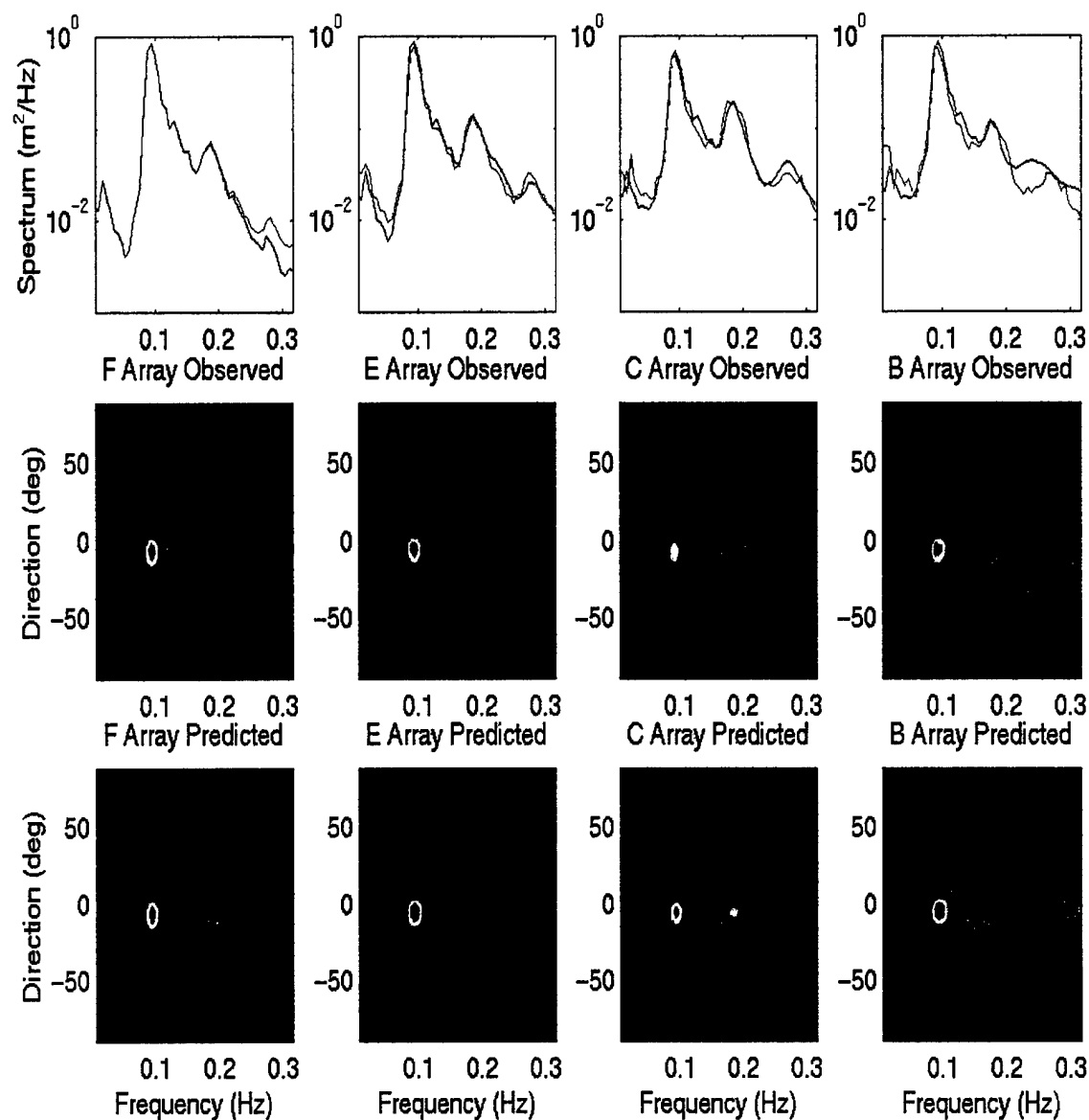


Figure 10. Frequency and frequency-directional spectra for Case II, (August 10, 1997 04:00 EST) (same format as figure 7).

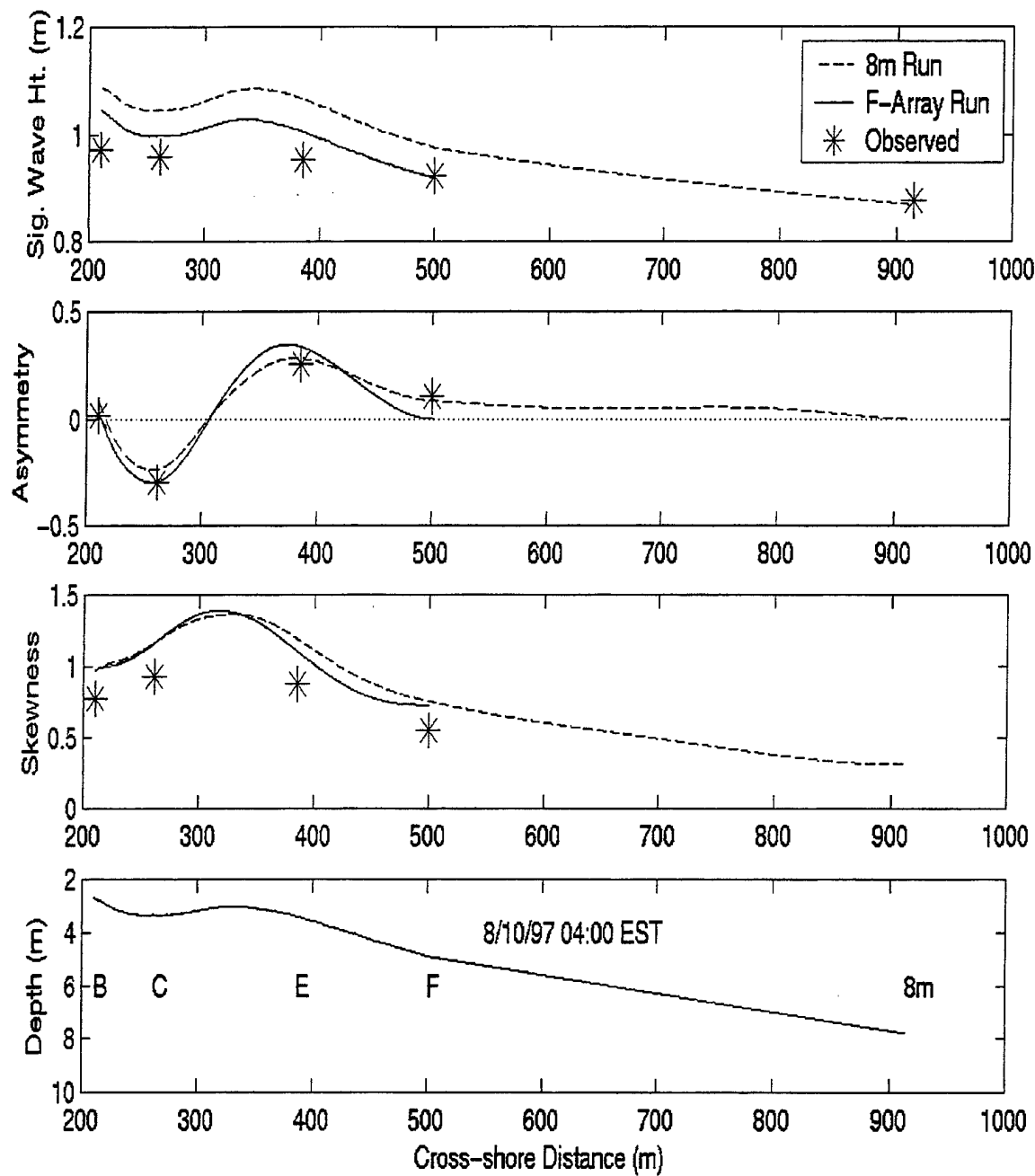


Figure 11. Case II, cross-shore shoaling evolution of significant wave height H_s , asymmetry, and skewness (same format as figure 8).

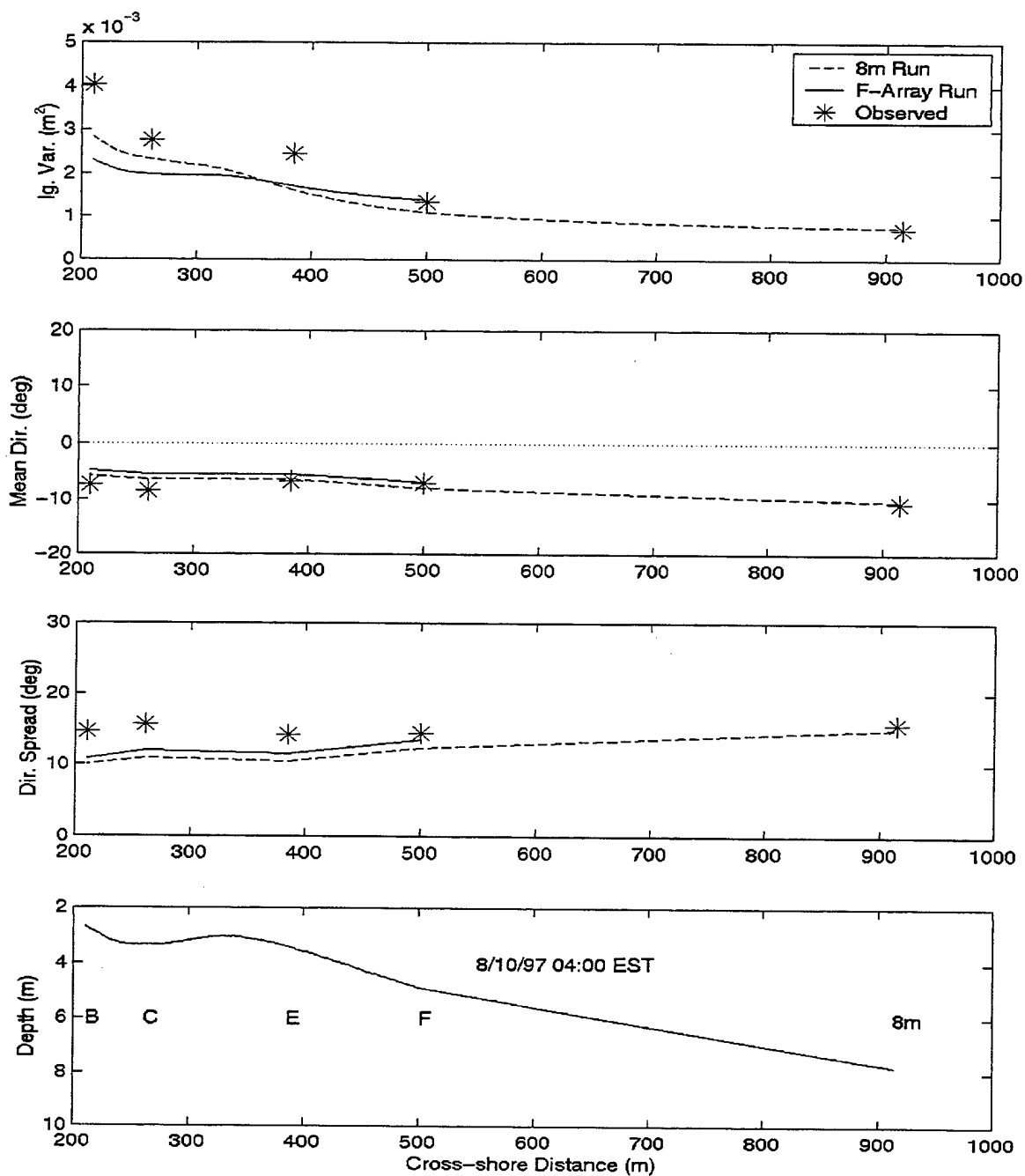


Figure 12. Case II, cross-shore shoaling evolution of infragravity variance, mean direction, and directional spread (same format as figure 9).

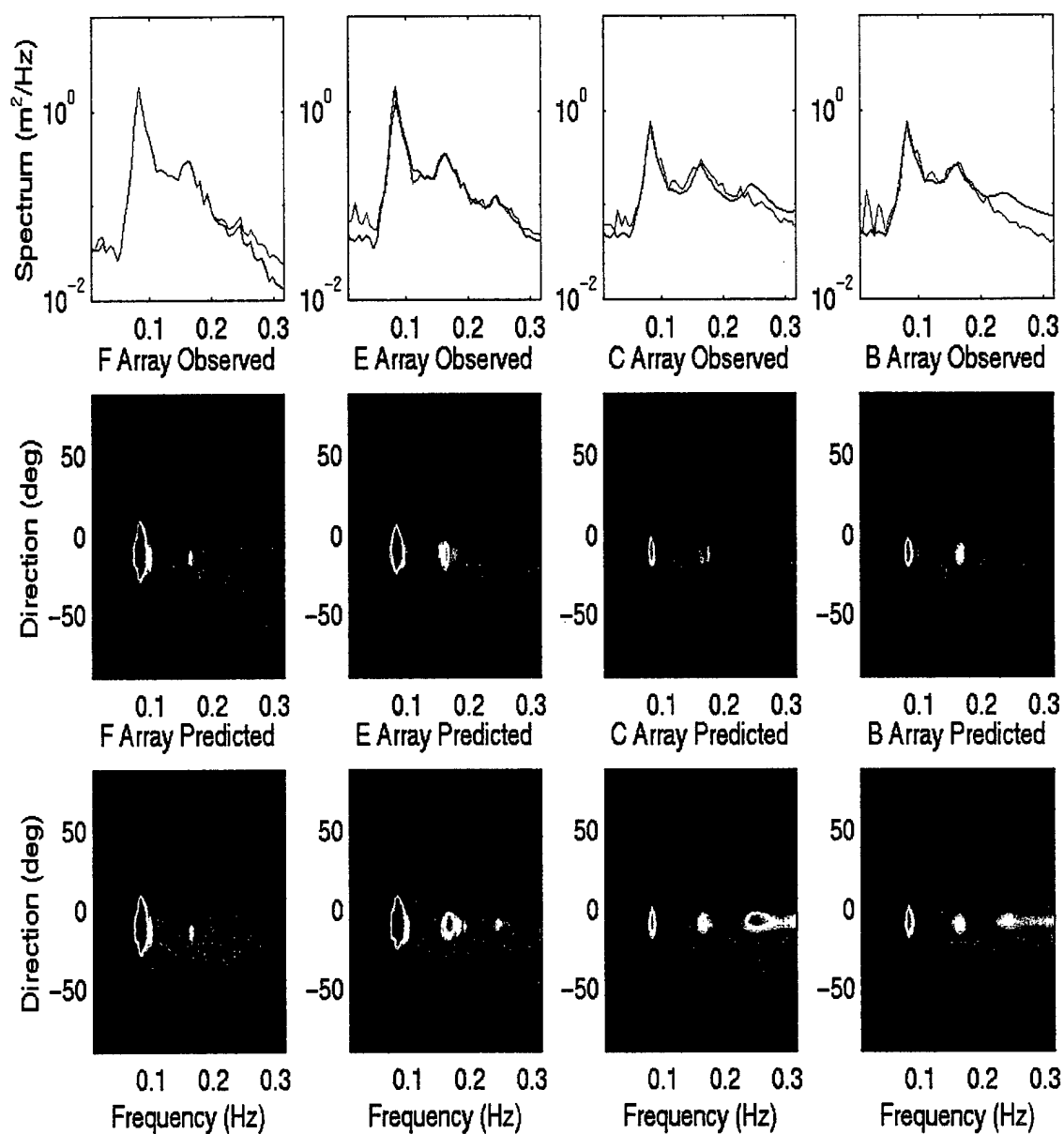


Figure 13. Frequency and frequency directional spectra for Case III (September 12, 1997 07:00 EST) (same format as figure 7). In order to enhance the directional properties at higher frequencies, the frequency-directional spectra (bottom two panels) were multiplied by the frequency.

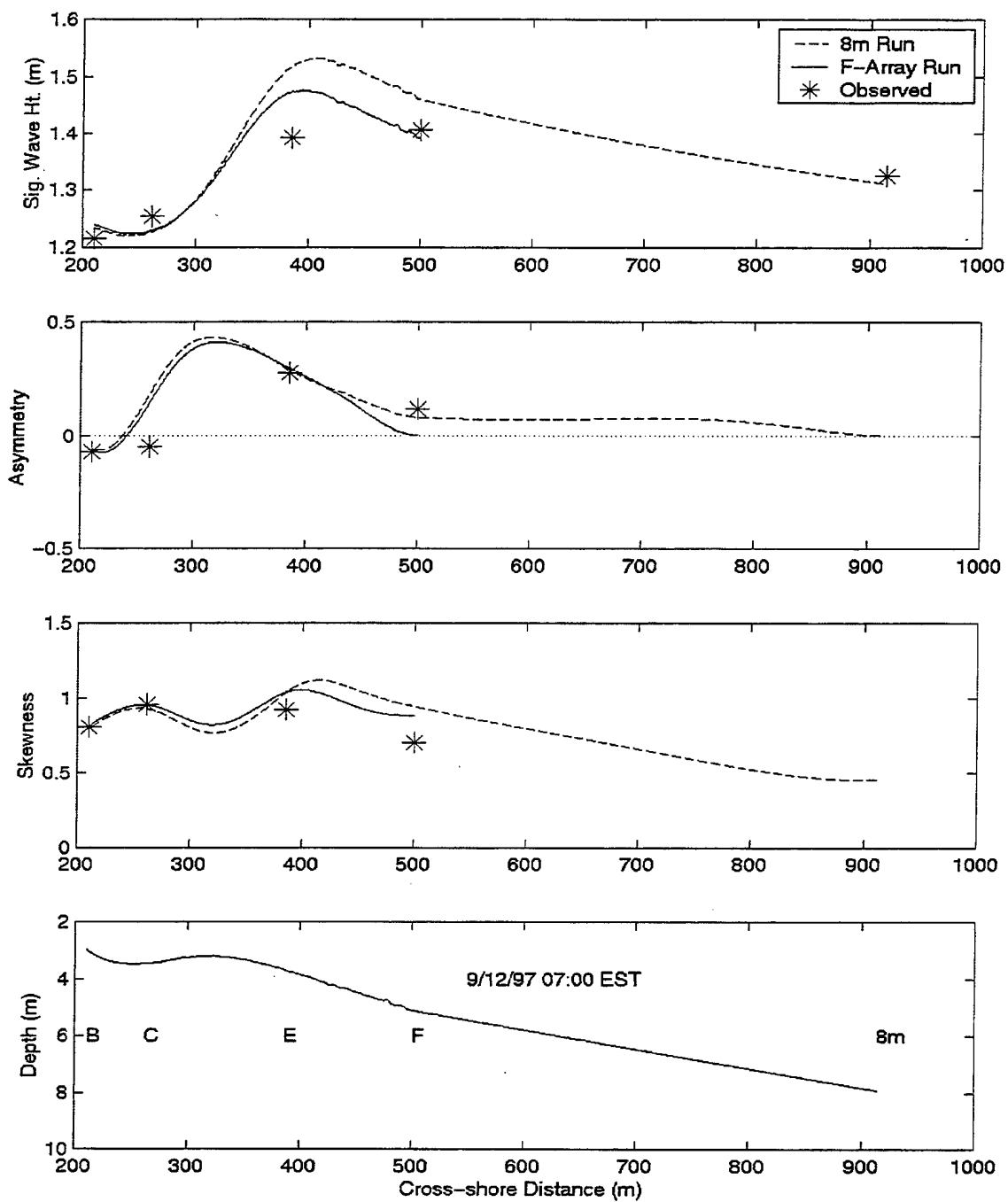


Figure 14. Case III, cross-shore shoaling evolution of significant wave height H_s , asymmetry, and skewness (same format as figure 8).

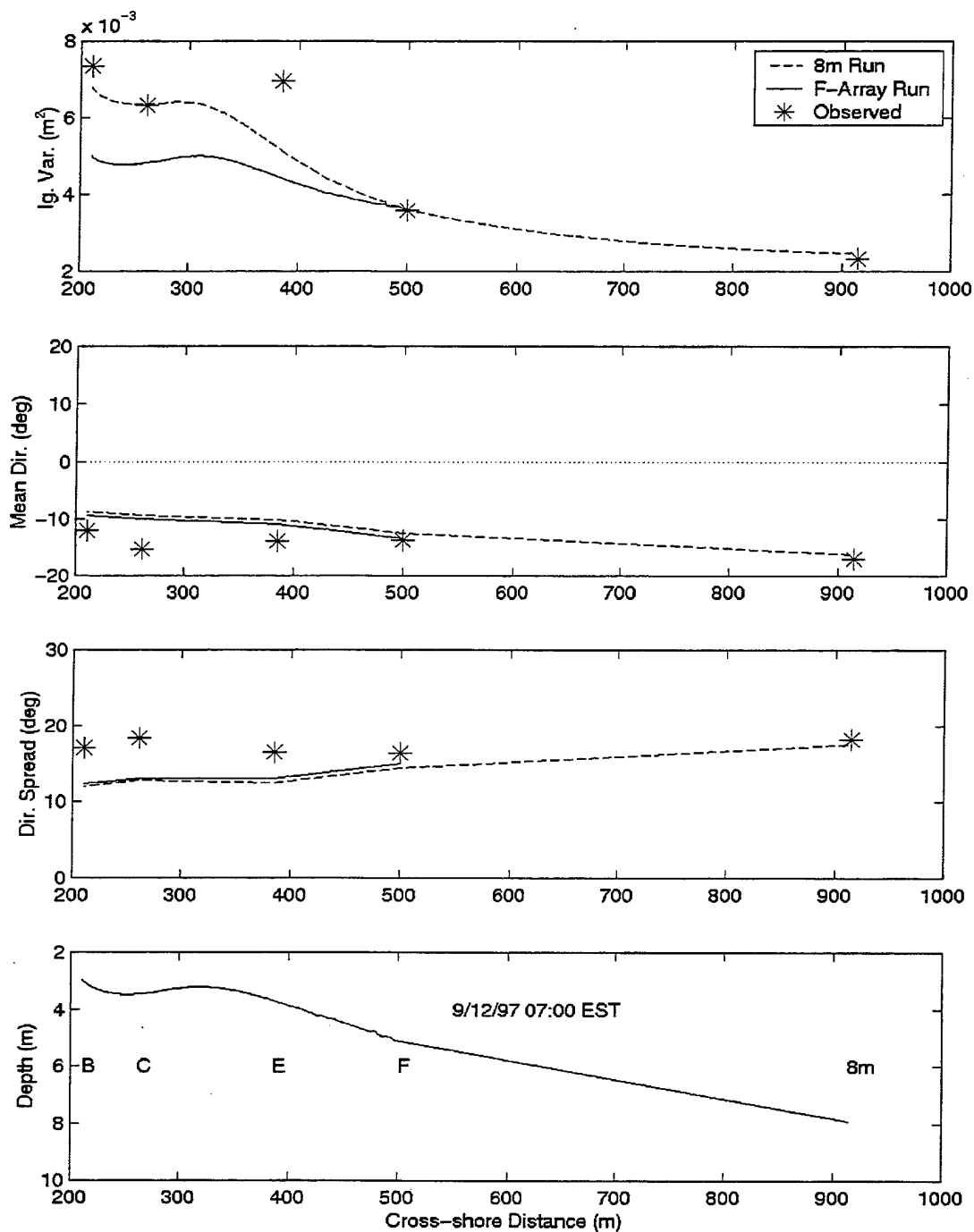


Figure 15. Case III, cross-shore shoaling evolution of infragravity variance, mean direction, and directional spread (same format as figure 9).

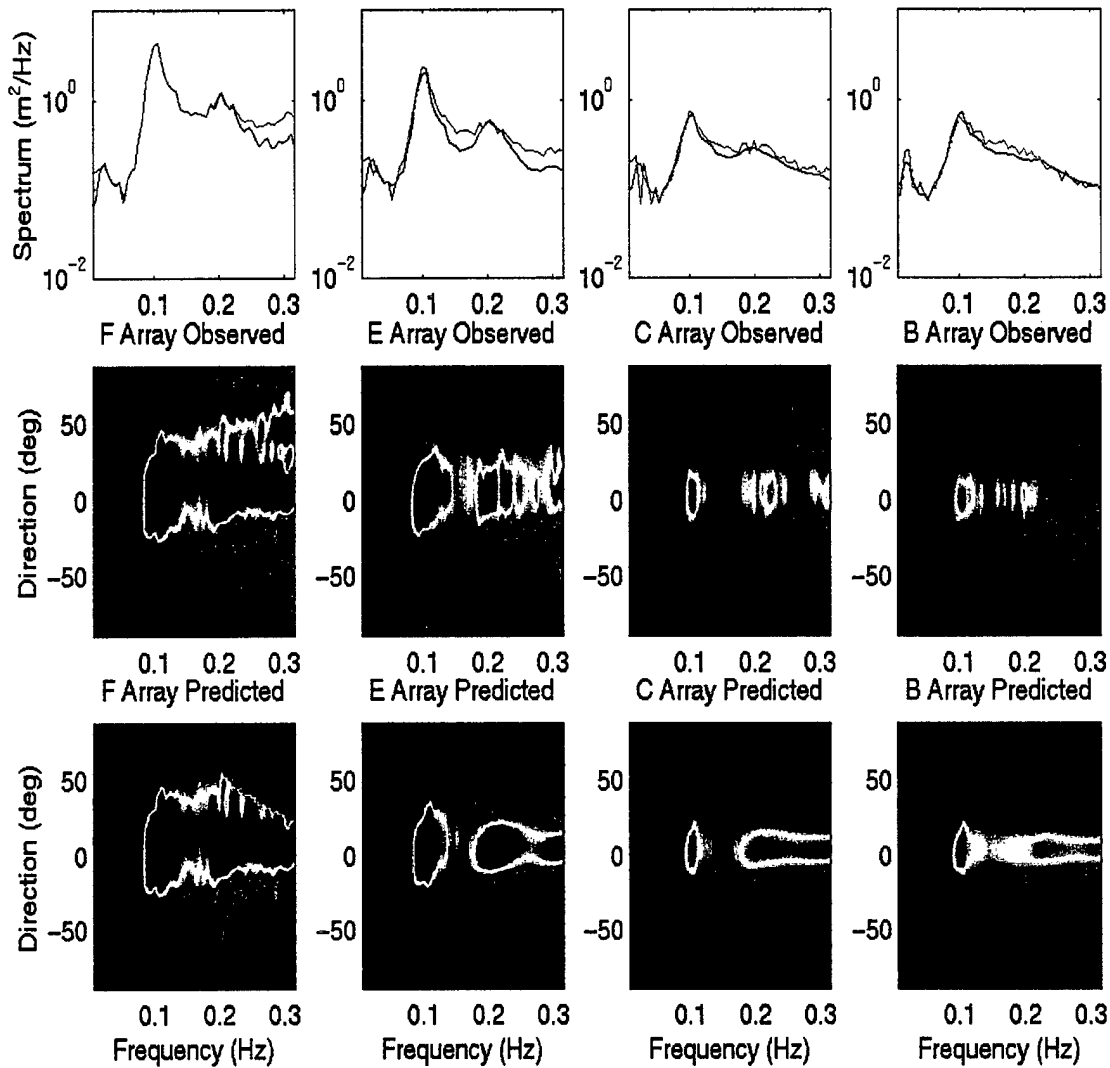


Figure 16. Frequency and frequency-directional spectra for Case IV (October 19, 1997 16:00 EST) (same format as figure 7). Note the exclusion of high frequency, large angle waves from the initializing model spectrum at the F array. In order to enhance the directional properties at higher frequencies, the frequency-directional spectra (bottom two panels) were multiplied by the frequency.

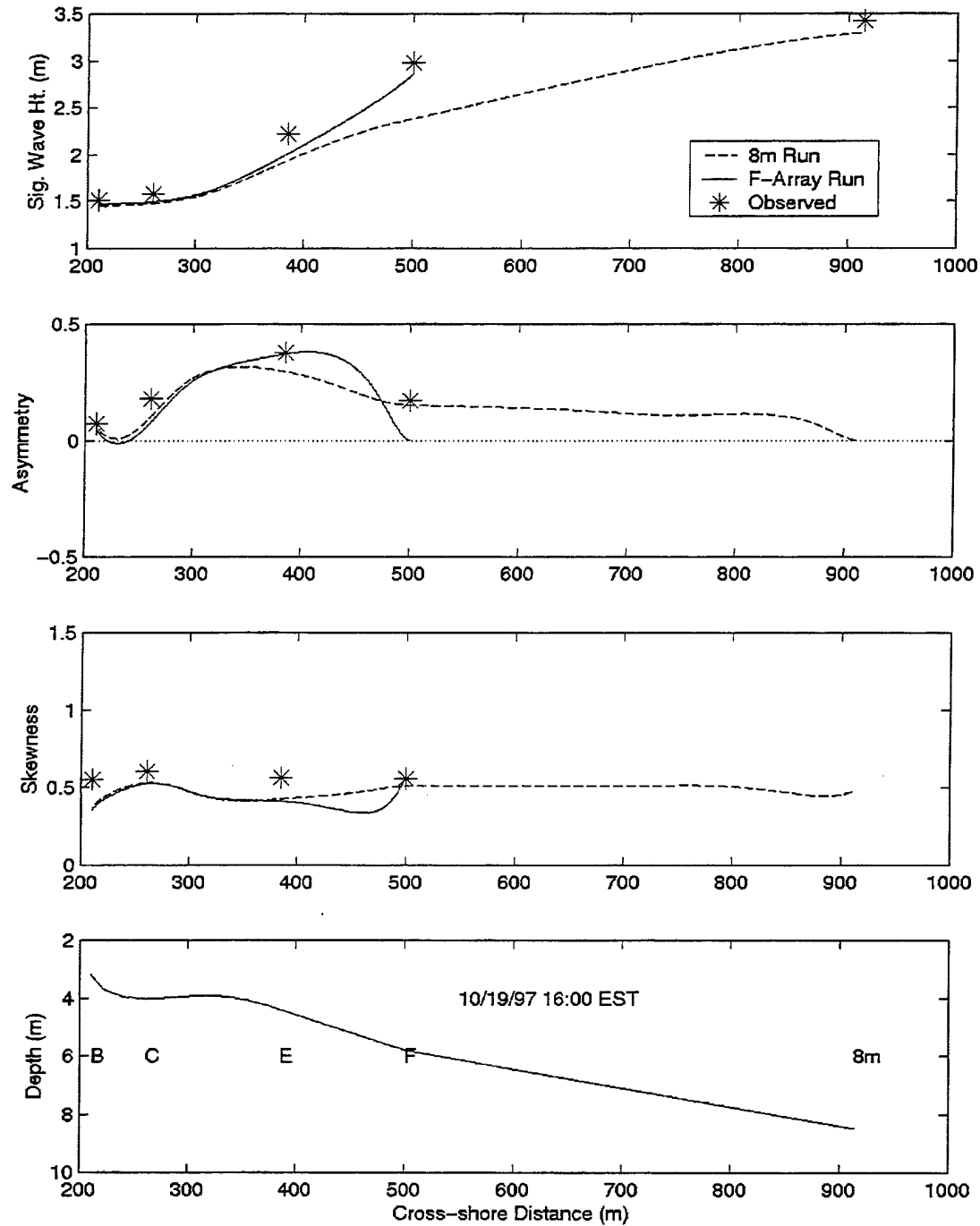


Figure 17. Case IV, cross-shore shoaling evolution of significant wave height H_s , asymmetry, and skewness (same format as figure 8).

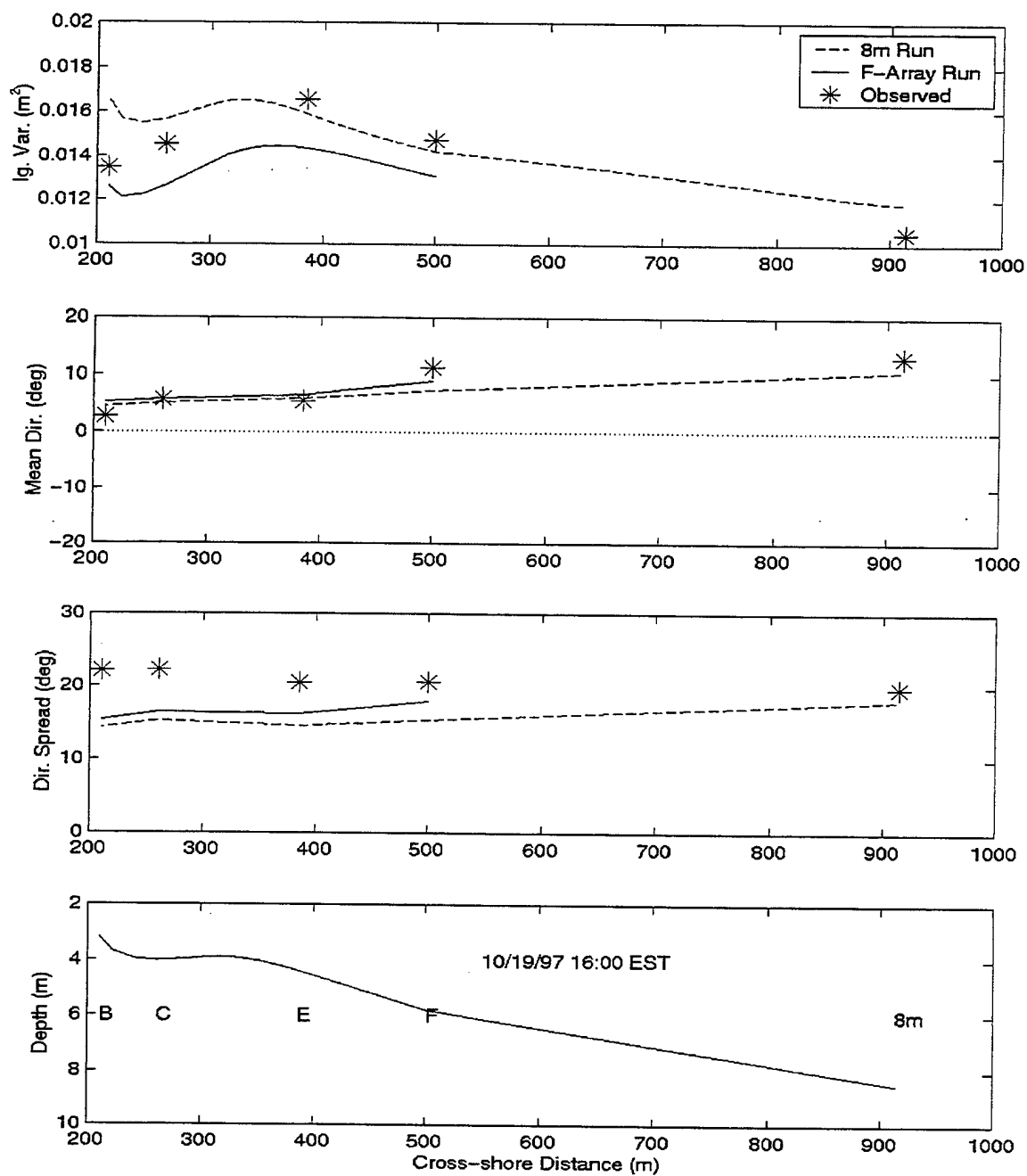


Figure 18. Case IV: cross-shore shoaling evolution of infragravity variance, mean direction, and directional spread (same format as figure 9).

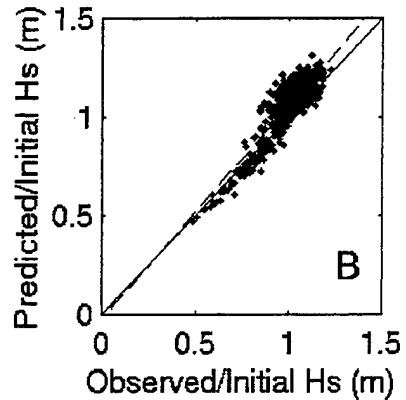
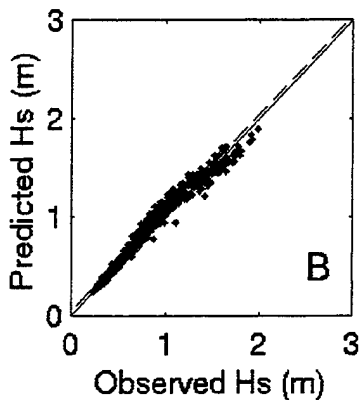
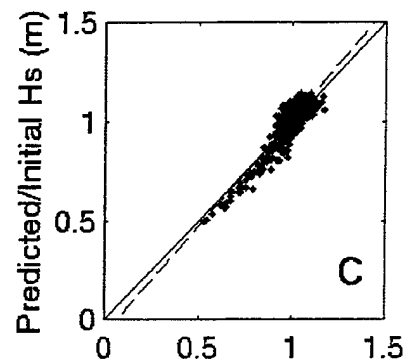
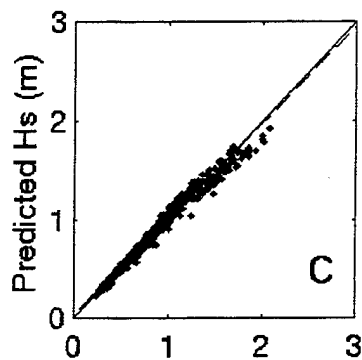
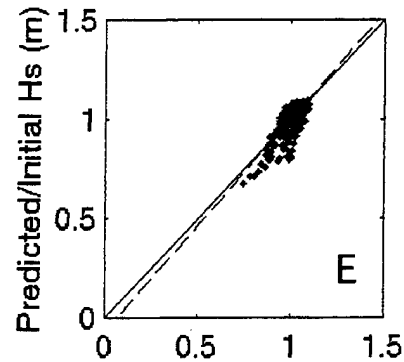
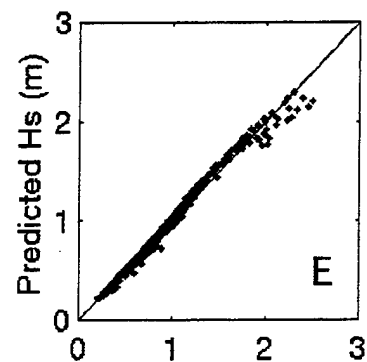


Figure 19. Left panels: predicted versus observed significant wave height (H_s) at the E, C, and B arrays. The model was initialized at the F array. Right panels: predicted versus observed significant wave height (H_s) both normalized by the initial H_s value. Solid diagonal line indicates a one-to-one correspondence, dashed line is a linear regression fit to all data points.

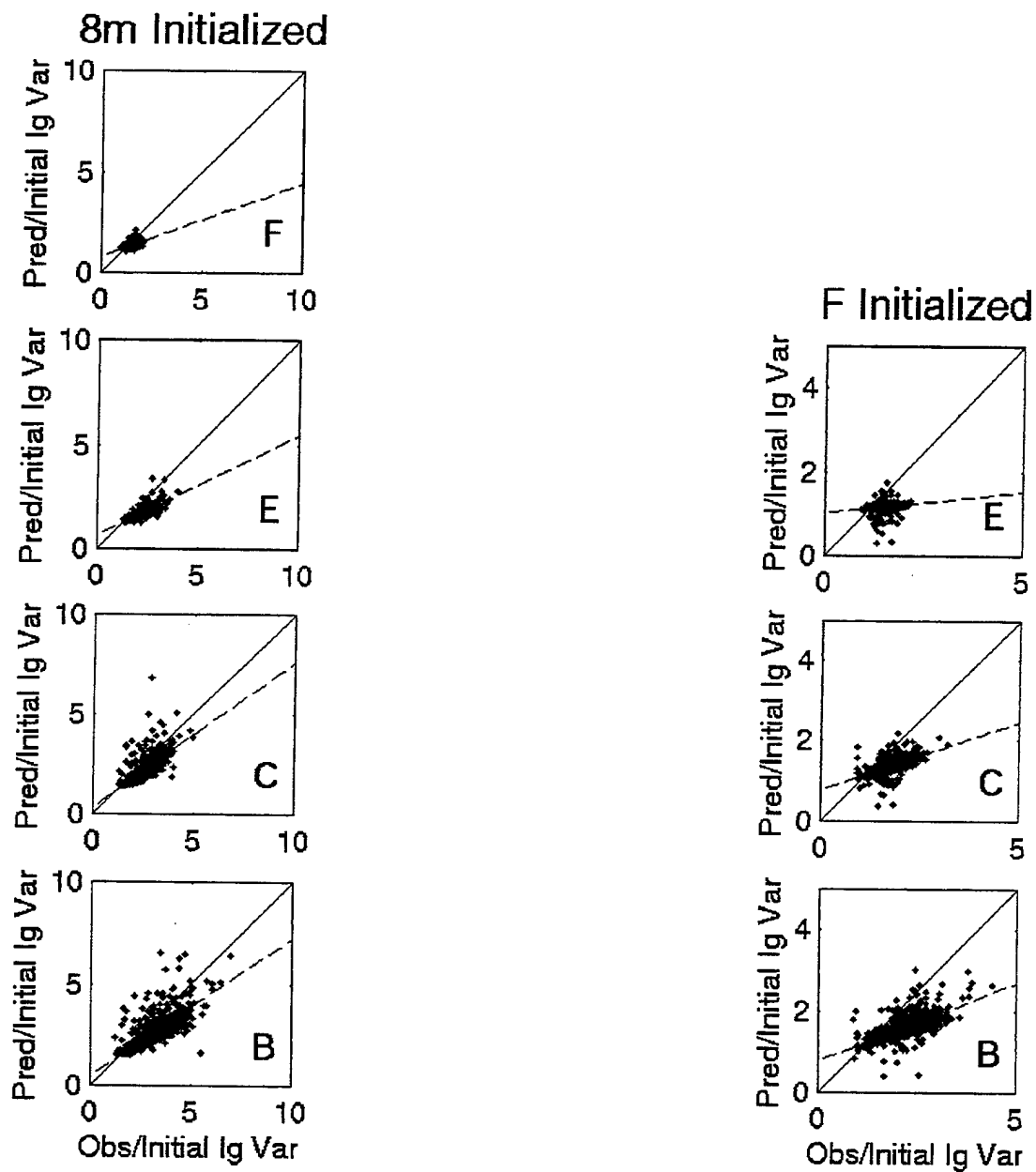


Figure 20. Predicted versus observed infragravity variance, both normalized by the initial infragravity variance. Left panels: results at the F, E, C, and B arrays for model runs initialized at the 8m array. Right panels: results at the E, C, and B arrays for model runs initialized at the F array. Solid diagonal line indicates a one-to-one correspondence, dashed line is a linear regression fit to all data points.

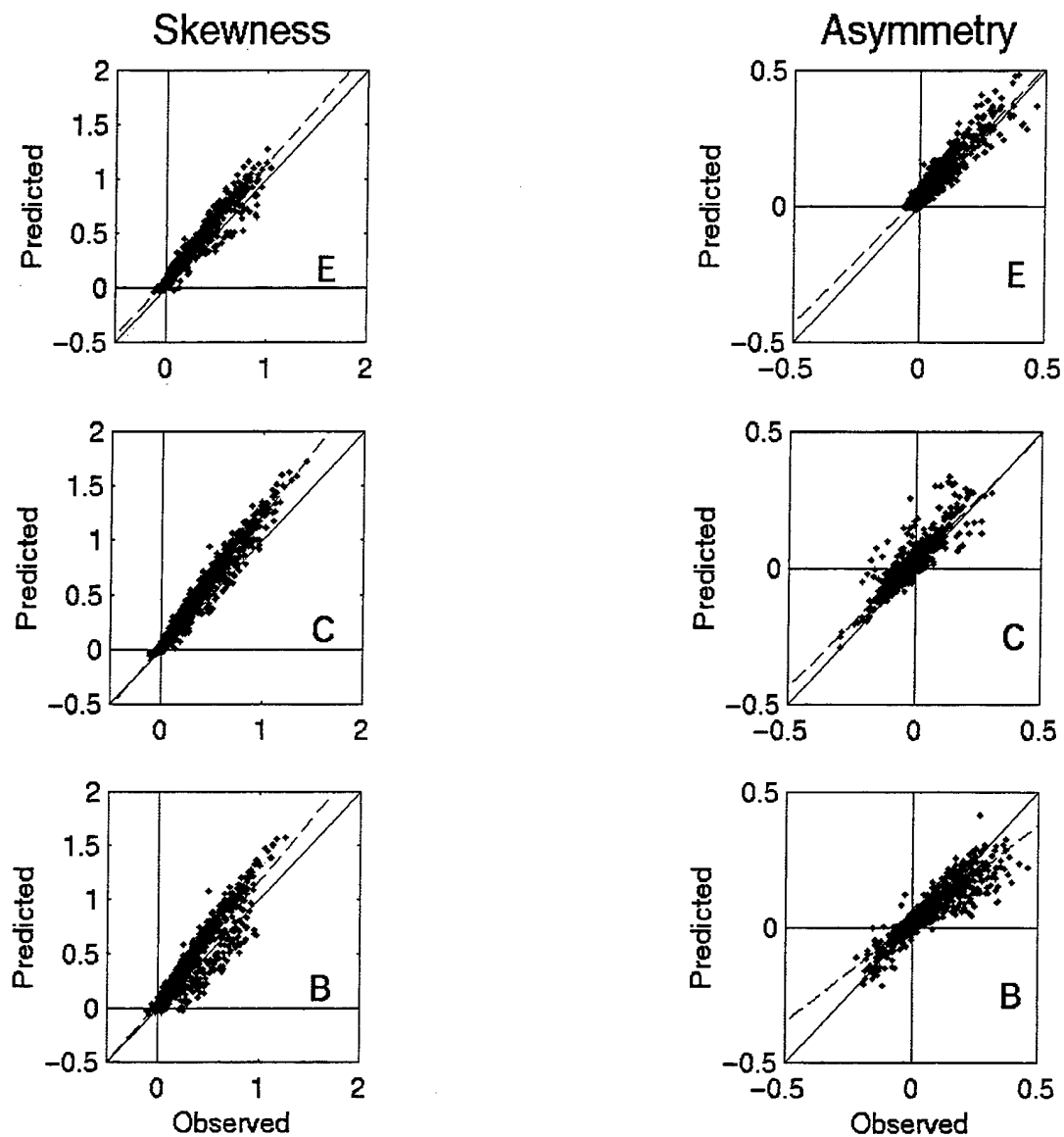


Figure 21. Predicted versus observed skewness (left panels) and asymmetry (right panels) at the E, C, and B arrays. The model was initialized at the F array. Solid diagonal line indicates a one-to-one correspondence, dashed line is a linear regression fit to all data points.

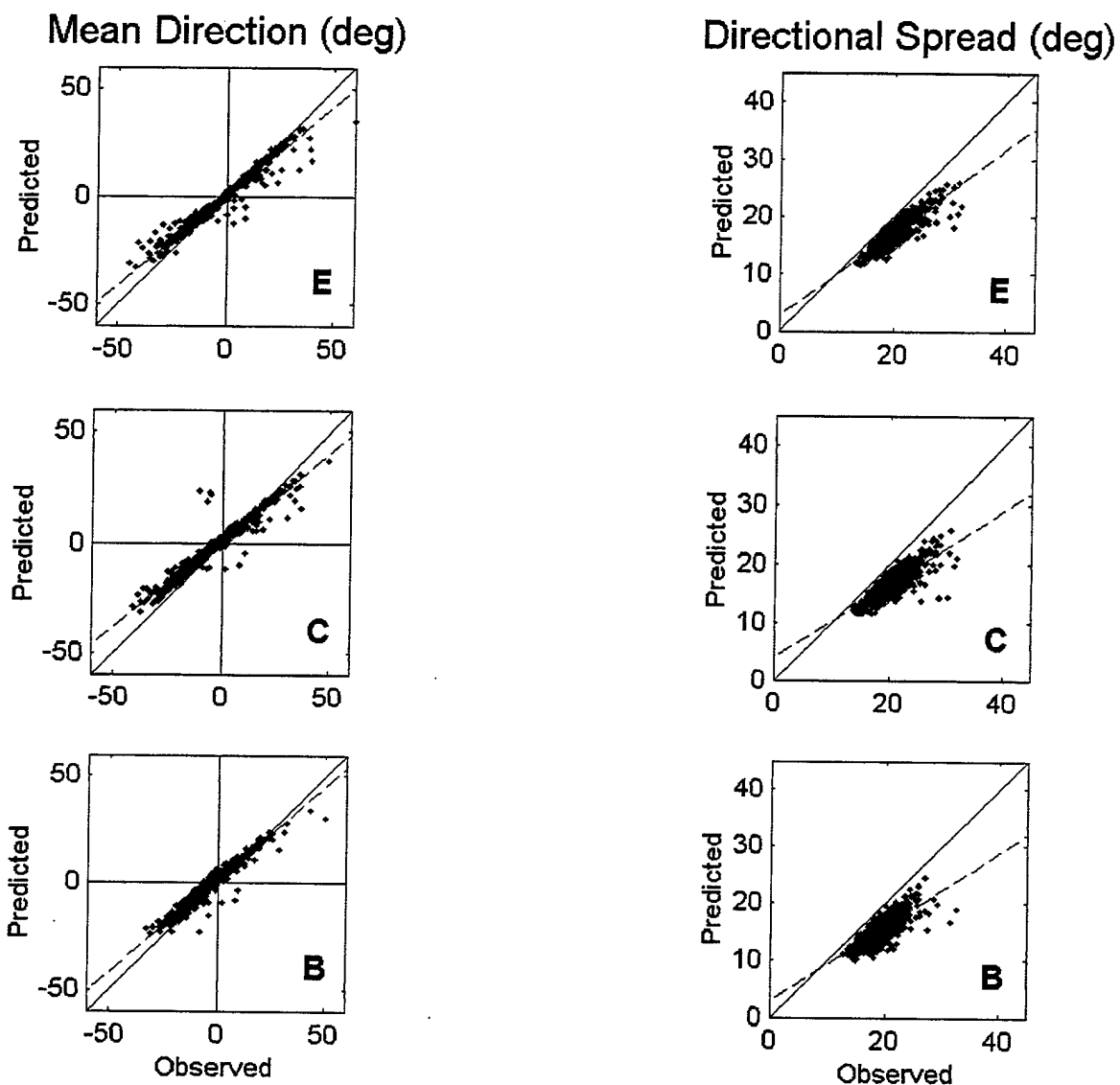


Figure 22. Predicted versus observed mean direction (left panels) and directional spread (right panels) at the E, C, and B arrays. The model was initialized at the F array. Solid diagonal line indicates a one-to-one correspondence, dashed line is a linear regression fit to all data points.

8m Model Run	Bias	RMS Error	Scatter Index	Correlation Coef.
Hs	0.047 m	0.081 m	0.092	0.986
Asymmetry	0.014	0.04	0.43	0.903
Skewness	0.105	0.144	0.37	0.949
Infragravity Variance	-0.00018 m ²	0.00056 m ²	0.19	0.976
Mean Direction	1.4 deg	5.9 deg	0.4	0.915
Directional Spread	-3.9 deg	4.3 deg	0.21	0.792

Table 1. Error statistics for model predictions initialized at the 8m array. Results are included from the F,E,C, and B arrays.

F Model Run	Bias	RMS Error	Scatter Index	Correlation Coef.
Hs	0.021 m	0.055 m	0.063	0.991
Asymmetry	0.021	0.047	0.45	0.905
Skewness	0.105	0.145	0.34	0.947
Infragravity Variance	-0.00034 m ²	0.00070 m ²	0.21	0.98
Mean Direction	1.9 deg	3.8 deg	0.28	0.972
Directional Spread	-3.4 deg	3.8 deg	0.19	0.807

Table 2. Error statistics for model predictions initialized at the F array. Results are included from the E,C, and B arrays.

THIS PAGE INTENTIONALLY LEFT BLANK

LIST OF REFERENCES

- Abreu, M., A. Larraza, and E. Thornton, 1992: Nonlinear transformation of directional wave spectra in shallow water. *J. Geophys. Res.*, **97**, 15579-15589.
- Agnon, Y., and A. Sheremet, 1997: Stochastic nonlinear shoaling of directional spectra. *J. Fluid Mech.*, **345**, 79-99.
- Battjes, J. A. and J. P. F. M. Janssen, 1978: Energy loss and set-up due to breaking of random waves. *Proceedings of the 16th International Conference Coastal Engineering*, 569.
- Chen, Y., R. T. Guza, and S. Elgar, 1997: Modeling spectra of breaking surface waves in shallow water. *J. Geophys. Res.*, **102**, 25035-25046.
- Eldeberky, Y., and J. A. Battjes, 1996: Spectral modeling of wave breaking: Application to Boussinesq equations. *J. Geophys. Res.*, **101**, 1253-1264.
- Elgar, S., and R. T. Guza, 1985b: Observations of bispectra of shoaling surface gravity waves. *J. Fluid Mech.*, **161**, 425-448.
- Elgar, S., R. T. Guza, and M.H. Freilich, 1993: Observations of nonlinear interactions in directionally spread shoaling surface gravity waves. *J. Geophys. Res.*, **98**, 20299-20305.
- Elgar, S., T. H. C. Herbers, and R. T. Guza, 1994: Reflection of ocean surface gravity waves from a natural beach. *J. Phys. Oceanogr.*, **24**, 1503-1511.
- Elgar, S., R. T. Guza, W. C. O'Reilly, B. Raubenheimer, and T. H. C. Herbers, 2001: Wave energy and direction observed near a pier. *J. Waterway, Port, Coastal, and Ocean Eng.*, **127**, 2-6.
- Freilich, M. H., and R. T. Guza, 1984: Nonlinear effects on shoaling surface gravity waves. *Phil. Trans. R. Soc. Lond.*, **A311**, 1-41.
- Freilich, M.H., Guza, R.T. and Elgar, S., 1990: Observations of nonlinear effects in directional spectra of shoaling gravity waves. *J. Geophys. Res.*, **95**, 9645-9656.
- Feddersen, F., R. T. Guza, S. Elgar, and T. H. C. Herbers, 2000: Velocity moments in alongshore bottom stress parameterizations, *J. Geophys. Res.*, **105**(C4), 8673-8686.
- Hasselmann, K., W. Munk, and G. MacDonald, 1963: Bispectra of ocean waves. *Times Series Analysis*, edited by M.R. Rosenblatt, John Wiley, New York, 125-139.
- Herbers, T. H. C. and R. T. Guza, 1990: Estimation of Directional Wave Spectra from Multicomponent Observations. *J. Phys. Oceanogr.*, **20**, 1703-1724.

- Herbers, T. H. C., and M. C. Burton, 1997: Nonlinear shoaling of directionally spread waves on a beach. *J. Geophys. Res.*, **102**, 21101-21114.
- Herbers, T. H. C., Elgar, S., and Guza, R. T., 1999: Directional spreading of waves in the nearshore, *J. Geophys. Res.*, **104**, 7683-7693.
- Mase, H., and J. T. Kirby, 1992: Hybrid frequency-domain KdV equation for random wave transformation, in *Proceedings of 23rd International Conference on Coastal Engineering*, pp. 474-487, American Society of Civil Engineers, New York.
- Norheim, C. A., T. H. C. Herbers, and S. Elgar, 1998: Nonlinear evolution of surface wave spectra on a beach. *J. Phys. Oceanogr.*, **28**, 1534-1551.
- Peregrine, D. H., 1967: Long waves on a beach. *J. Fluid Mech.*, **27**, 815-827.
- Thornton, E. B., and R. T. Guza, 1982: Energy saturation and phase speeds measured on a natural beach. *J. Geophys. Res.*, **87**, 9499-9508.
- Whitford, D. J., 1988: Wind and wave forcing of longshore currents across a barred beach, Ph.D. Thesis, Naval Postgraduate School, Monterey, CA.

INITIAL DISTRIBUTION LIST

1. Defense Technical Information Center2
 8725 John J. Kingman Road, Suite 0944
 Ft. Belvoir, VA 22060-6218

2. Dudley Knox Library2
 Naval Postgraduate School
 411 Dyer Road
 Monterey, CA 93943-5101

3. Professor T.H.C. Herbers, Code OC/He7
 Department of Oceanography
 Naval Postgraduate School
 Monterey, CA 93943-5121

4. Professor E.B. Thornton, Code OC/Tm1
 Department of Oceanography
 Naval Postgraduate School
 Monterey, CA 93943-5121

5. Mark Orzech, Code OC/OH1
 Department of Oceanography
 Naval Postgraduate School
 Monterey, CA 93943-5121

6. Marianie O. Balolong2
 2457 Seymour Street
 Jacksonville, FL 32246